Shape and Dynamics of Adhesive Cells: Mechanical Response of Open Systems

Yuehua Yang and Hongyuan Jiang*
CAS Key Laboratory of Mechanical Behavior and Design of Materials, Department of Modern Mechanics, University of Science and Technology of China, Hefei, Anhui 230027, China
(Received 4 October 2016; published 19 May 2017)

Cell adhesion is an essential biological process. However, previous theoretical and experimental studies ignore a key variable, the changes of cellular volume and pressure, during the dynamic adhesion process. Here, we treat cells as open systems and propose a theoretical framework to investigate how the exchange of water and ions with the environment affects the shape and dynamics of cells adhered between two adhesive surfaces. We show that adherent cells can be either stable (convex or concave) or unstable (spontaneous rupture or collapse) depending on the adhesion energy density, the cell size, the separation of two adhesive surfaces, and the stiffness of the flexible surface. Strikingly, we find that the unstable states vanish when cellular volume and pressure are constant. We further show that the detachments of convex and concave cells are very different. The mechanical response of adherent cells is mainly determined by the competition between the loading rate and the regulation of the cellular volume and pressure. Finally, we show that as an open system the detachment of adherent cells is also significantly influenced by the loading history. Thus, our findings reveal a major difference between living cells and nonliving materials.

DOI: 10.1103/PhysRevLett.118.208102

Adhesion of cells to an extracellular matrix or another cell plays a fundamental role in many physiological processes, such as cell migration, wound healing, cell recognition, and rigidity sensing [1–5]. The adhesion strength and the rupture force are the key parameters to characterize cell adhesion. Consequently, the quantitative measurement of these properties of adhesive cells is essential for understanding the fundamental mechanisms of the adhesion-related processes and phenomena.

With the development of experimental techniques, such as micropipette aspiration [6–8], atomic force microscopy [9,10], optical tweezing [11], and microplate manipulation [12–16], the properties of cell adhesion and cell deformability have been extensively explored experimentally. Conventionally, the extraction of these properties from experimental data is mostly based on contact mechanics models [17,18], the Young-Dupré equation [6,19], or the model proposed by Brochard-Wyart and de Gennes [20–22]. In these models, cell volume is either assumed to be constant or totally ignored. However, when cells suffer from large deformation, cell volume, cortical tension, and hydrostatic pressure usually change dramatically [23–29] due to the extensive exchange of water and ions with the environment. For example, cell volume can increase by 30% during the mitotic cell rounding from the adherent state [25], and decrease by 30% under shear stress [26,27]. Cell volume can also change more than 40% due to osmotic shocks [28,29]. However, in such a nonequilibrium open system, how the shape and dynamics of adherent cells are affected by the cellular volume and pressure regulation is still elusive.

To answer this question, we focus on cells adhered symmetrically between two surfaces (Fig. 1) as frequently used in atomic force microscope, microplate manipulation, and micropipette aspiration experiments. One adhesive surface can be treated as a rigid body, and the other can be regarded as a cantilever with an equivalent spring stiffness [Fig. 1(c)]. First, the fixed end of the cantilever is moved downward d_0 to compress a spherical cell with an

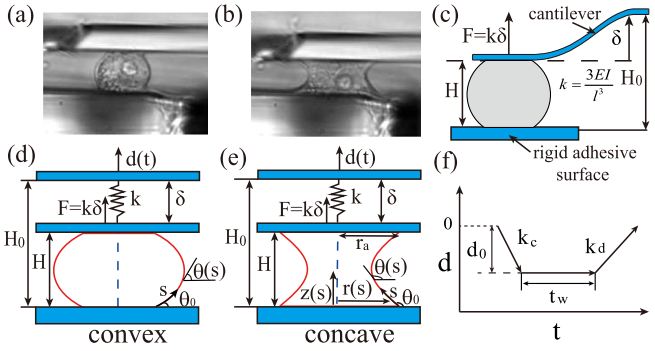

FIG. 1. Schematic of cells adhered symmetrically between an adhesive surface and a cantilever. Panels (a) and (b) show convex and concave cells observed in experiments (adapted from Ref. [15] with permission). (c) The deflection of the cantilever is $\delta = Fl^3/3EI$, where F is the force applied by the cell and EI is the bending stiffness of the cantilever. Thus, the cantilever can be treated as a spring with a stiffness of $k = 3EI/l^3$ and zero rest length. In (d) and (e), the cell shape is cylindrically symmetric and can be described by $r(s)$ and $z(s)$, where s is the arc length. $\theta(s)$ is the tangential angle of the arc length, and θ_0 is the contact angle. So the cell is convex when $\theta_0 < 90°$ and concave when $\theta_0 > 90°$. r_a is the adhesion radius. H is the cell height and H_0 is the separation of the adhesive surface and cantilever. $d(t)$ is the displacement of the fixed end of the cantilever. (f) The loading and unloading process.

initial radius of r_0 [Fig. 1(f)]. Then, we stop and hold the cantilever for a duration of t_w. After the waiting time t_w, the cell becomes either convex [Fig. 1(a)] or concave [Fig. 1(b)] due to adhesion, although the cell is always convex initially. Finally, the cantilever is moved upward at a speed k_d to induce detachment [Fig. 1(f)].

We treat cells as open systems, i.e., water and ions can pass through the cell membrane passively or actively. Therefore, the time evolution of the cellular volume V and the total number of ions n due to the transport of water and ions are [23]

$$\frac{dV}{dt} = -L_p A_{\mathrm{eff}}(\Delta P - \Delta\Pi), \tag{1}$$

$$\frac{dn}{dt} = A_{\mathrm{eff}}(J_{\mathrm{out}} + J_{\mathrm{in}}), \tag{2}$$

where A_{eff} is the effective surface area, i.e., the difference between the total surface area and the adhesion area. L_p is the membrane permeability rate to water. ΔP and $\Delta\Pi$ are the hydrostatic and osmotic pressure differences, respectively. J_{out} reflects the ion efflux due to the opening of passive mechanosensitive channels. J_{in} describes the influx of ions through ion pumps that actively pump ions into the cell. More details of the model are specified in the Supplemental Material [30].

The cell is surrounded by the cortical layer and cell membrane. Therefore, both the cortical tension T_{cortex} and membrane tension T_m contribute to the total surface tension T_s, i.e., $T_s = T_{\mathrm{cortex}} + T_m$ [63,64]. The cortical layer is modeled as a fluidlike layer with a constant active stress σ_a [65]. The stress in the cortical layer σ_{cortex} is described by $\sigma_{\mathrm{cortex}} = \eta\dot{\varepsilon}_A + \sigma_a$ [66], where $\dot{\varepsilon}_A$ is the strain rate of the cellular surface area and η is the viscosity of the cortical layer. Thus, the cortical tension is $T_{\mathrm{cortex}} = \sigma_{\mathrm{cortex}} h_c$, where h_c is the thickness of the cortical layer. The membrane tension is related to the membrane stress σ_m by $T_m = \sigma_m h_m$, where h_m is the membrane thickness. We can consider an equivalent surface stress σ in these two layers as $T_s = \sigma h$, where $h = h_m + h_c$. Therefore, the surface stress can be determined by $\sigma(h_m + h_c) = \sigma_{\mathrm{cortex}} h_c + \sigma_m h_m$. We can use a membrane reservoir model or a viscoelastic model to describe the membrane stress (see the Supplemental Material [30] for details), but we find the results of these two models are qualitatively the same (Figs. S3 and S5 of Ref. [30]). So we use the reservoir model for the simulations in the main text.

The force balance yields

$$2\pi\sigma h r \sin\theta = \Delta P \pi r^2 + F, \tag{3}$$

where θ is the tangential angle of the arc length, r is the cell radius, and F is the external force applied by the cantilever (Fig. 1). Notice that F is positive when the cell is stretched.

The contact angle θ_0 defined in Figs. 1(d) and 1(e) is given by the Young-Dupré equation as

$$\Gamma = \sigma h(1 - \cos\theta_0), \tag{4}$$

where Γ is the adhesion energy density between the cell and substrate. When $\Gamma = 0$, Eq. (4) is reduced to $\theta_0 = 0$, which is the situation discussed previously [23]. In general, Γ can vary with time due to the binding and unbinding of the ligand-receptor bonds. The time evolution of Γ is (see the Supplemental Material [30] for details)

$$\frac{d\Gamma}{dt} = \Gamma_0 k_{\mathrm{off}}^0 \left[1 - \frac{\Gamma}{\Gamma_0}\exp\left(\frac{aFV_e}{k_B T \Gamma \pi r_a^2}\right)\right], \tag{5}$$

where Γ_0 is the equilibrium adhesion energy density when $F = 0$, and k_{off}^0 is the dissociation rate of ligand-receptor pairs when $F = 0$. r_a is the adhesion radius, a is the characteristic length of the bond deformation, V_e is the rupture energy of a single bond [67], k_B is Boltzmann's constant, and T is the absolute temperature. Notice that at the steady state ($d\Gamma/dt = 0$), the equilibrium adhesion energy density Γ_s for nonzero F depends on the external force, i.e., $F = (k_B T \Gamma_s \pi r_a^2/aV_e)\ln(\Gamma_0/\Gamma_s)$.

First, we consider the dynamic adhesion with constant H_0 (the end of the cantilever is fixed). Here, we assume Γ_0 is very small (weak adhesion) and the waiting time t_w defined in Fig. 1(f) is long enough so that the cell has already reached the steady state. Then, we suddenly increase Γ_0 to find a new steady state. In this case, the contact angle θ_0 and adhesion radius r_a increase with time [Fig. 2(a), and Fig. S8 of Ref. [30]]. Meanwhile, the tip of the cantilever moves downward so that cell height H decreases and F increases until the cell reaches its new steady state.

For small Γ_0, we find the steady cell shape is convex ($\theta_0 < 90°$), but the cantilever can apply a pulling ($F > 0$) or pushing ($F < 0$) force [Fig. 2(a), and Movies S1 and S2 of Ref. [30]]. For large Γ_0, the cell undergoes a transition from a convex shape to a concave shape as $\Gamma(t)$ increases with time [light green curve in Fig. 2(a), subplot (II), and Movie S3 of Ref. [30]], and F changes from a pushing force to a pulling force. Therefore, there is a critical Γ_0, above which the steady adherent cell is concave ($\theta_0 > 90°$). Besides Γ_0, we find the separation between the two adhesive surfaces H_0 can also affect the steady cell shape. The cell is more likely to be concave for larger H_0, as shown in the phase diagram [Fig. 3(a)].

Interestingly, we find that the steady cell shape depends not only on Γ_0 and H_0, but also on the initial cell size r_0, i.e., the radius of the spherical cells in suspension. If we decrease r_0 from 18 μm [Fig. 3(a)] to 10.5 μm [Fig. 3(b)], another region appears in the phase diagram [dark green region in Fig. 3(b), and Movie S4 in Ref. [30]], where the "spontaneous rupture" of cells occurs due to the

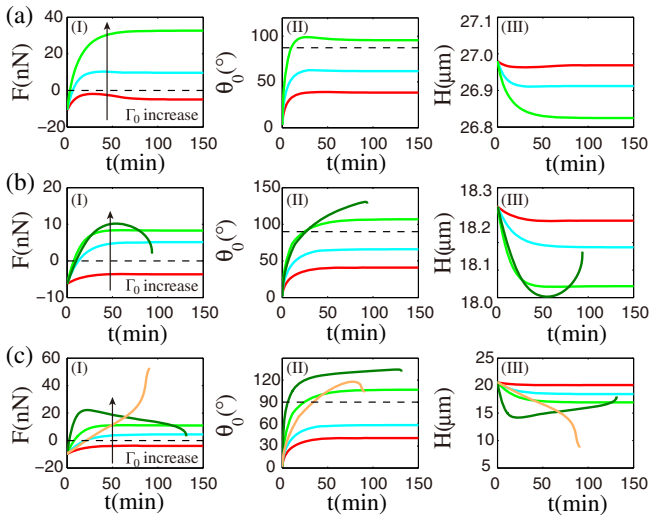

FIG. 2. Dynamic adhesion of cells adhered to an adhesive surface and a cantilever. (a) $r_0 = 18\ \mu$m, $k = 0.5$ N/m; (b) $r_0 = 10.5\ \mu$m, $k = 0.5$ N/m; (c) $r_0 = 10.5\ \mu$m, $k = 0.01$ N/m. The parameters H_0 and Γ_0 used here are marked by stars in Fig. 3. Other parameters are the same (Table S1 of Ref. [30]). The subplots show (I) external force F, (II) contact angle θ_0, and (III) cell height H. The red, light blue, and light green curves represent the dynamic process of reaching the three stable states: (1) the cell is convex ($\theta_0 < 90°$) and $F < 0$; (2) the cell is convex and $F > 0$; (3) the cell is concave ($\theta_0 > 90°$) and $F > 0$. The dark green and orange curves represent the spontaneous rupture and collapse of cells. The color of these curves corresponds to the color of the phase diagrams in Fig. 3. The dashed lines in subplots (I) and (II) indicate the lines of $F = 0$ and $\theta_0 = 90°$, respectively.

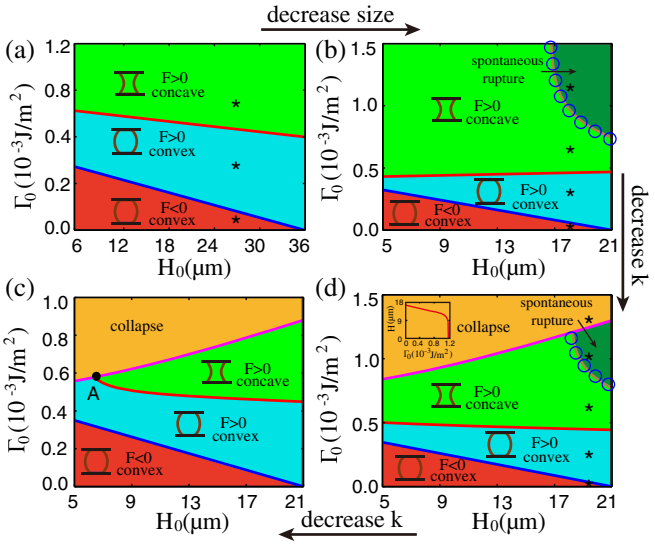

FIG. 3. Phase diagrams of cell shapes for various cantilever stiffnesses k and cell sizes r_0. (a) $r_0 = 18\ \mu$m, $k = 0.5$ N/m; (b) $r_0 = 10.5\ \mu$m, $k = 0.5$ N/m; (c) $r_0 = 10.5\ \mu$m, $k = 0.005$ N/m; (d) $r_0 = 10.5\ \mu$m, $k = 0.01$ N/m. There are three stable regions (red, light blue, and light green regions) and two unstable regions (dark green and orange regions). The stars indicate H_0 and Γ_0 used in Fig. 2. The blue circles in (b) and (d) are the theoretical predictions for the critical condition of the tension-induced rupture [30]. The inset in the orange region of (d) shows the collapse of the cell as Γ_0 increases.

adhesion-induced tension increases. The membrane tension increases rapidly and its time derivative is diverging at the time of rupture [dark green curves in Figs. S9(e) and S10(e) [30]]. In reality, when the tension is bigger than some critical value, the membrane and cortex will break. Here, because we did not consider the breakage of the membrane and cortex in the constitutive law, the membrane tension will keep increasing before cell rupture. This is similar to the rupture of red blood cells due to strong adhesion [68]. Mathematically, it indicates that for small cells there is a critical tension or cell height beyond which no catenoidlike solution exists [69]. The critical condition for the tension-induced rupture is given by Eq. (S48) in the Supplemental Material [30]. In this case, cell height H first decreases and then increases [dark green line in Fig. 2(b), subplot (III), and Movie S4 of Ref. [30]]. In contrast, F first increases and then decreases.

If the cantilever stiffness k decreases from 0.5 N/m [Fig. 3(b)] to 0.005 N/m [Fig. 3(c)], another region will emerge in the phase diagram [orange regions in Figs. 3(c) and 3(d), and Movie S5 of Ref. [30]]. In this case, the cell collapses to $H = 0$ when Γ_0 is large [inset in Fig. 3(d), orange region]. This is because under strong adhesion the cantilever is too soft to sustain the pulling force applied by the cell. Notably, the cell is easier to collapse for smaller H_0 [Figs. 3(c) and 3(d)]. Moreover, when k and H_0 are small enough, the cell may never become concave as Γ_0 increases. Instead, the cell will collapse at the convex stage [the left side of point A in Fig. 3(c)]. In fact, recent experiments found that when a cell spreads between a flexible microplate and a rigid microplate, the cell height can decrease to almost zero [15]. This is similar to but slightly different from the cell collapse we found here since the adhesion energy density used in the experiment is usually not very large and the occurrence of the full collapse may also be prevented by the resistance of cell organelles.

Strikingly, when cell volume is conserved during the spreading, the two unstable states (spontaneous rupture and collapse) vanish in the phase diagram (Fig. S11 [30]), and it is very hard for the cells to form a concave shape when k is small. Therefore, the regulation of cell volume and pressure directly induces the unique behaviors of spontaneous rupture and collapse we found here.

Now, we investigate the dynamic detachment of convex and concave cells. Here, we assume t_w is long enough so that the cell can reach the steady state after t_w (Fig. 1). Then, the fixed end of the cantilever is moved upward with a speed k_d to detach the cell. Here, we neglect the dynamics of Γ during detachment; i.e., Γ is constant, since we want to

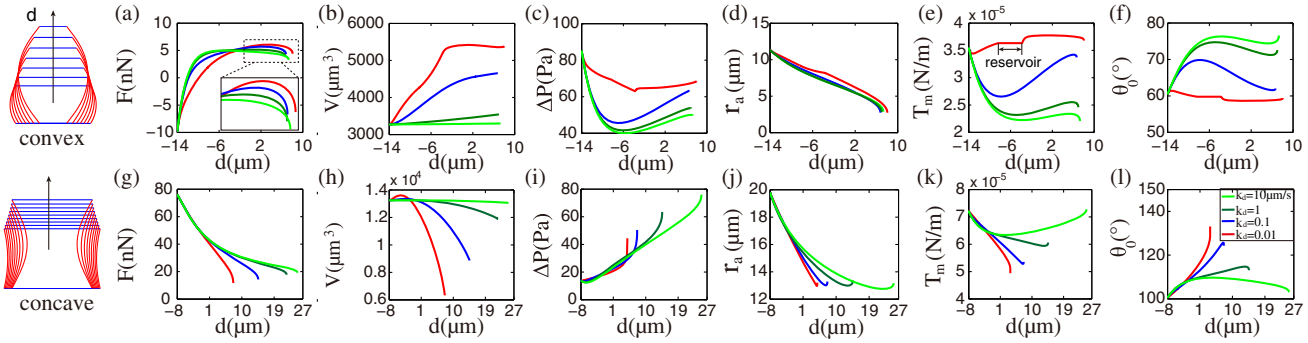

FIG. 4. Dynamic detachment of convex [(a)–(f)] and concave [(g)–(l)] cells that are initially at steady state; the initial compression is $d_0 = 14$ μm and $d_0 = 8$ μm for convex and concave cells, respectively. Left: the shape evolution during the detachment. The external force [(a),(g)], cellular volume [(b),(h)], hydrostatic pressure difference [(c),(i)], adhesion radius [(d),(j)], membrane tension [(e),(k)], and contact angle [(f),(l)] versus the displacement $d(t)$ with various loading speeds k_d.

focus on how cell volume regulation influences cell detachment. For convex cells, F first increases and then decreases slowly after reaching its maximum as the displacement d increases [Fig. 4(a)]. At steady state, there are two types of convex cells ($F < 0$ or $F > 0$). So F could be negative or positive initially. However, we find that the detachment processes of these two kinds of convex cells are qualitatively the same (Fig. S12 [30]). For concave cells, however, F is always positive and F decreases as d increases [Fig. 4(g)], which is very similar to the rupture of liquid bridges [70–73].

We find that the response of cells greatly depends on the loading rate k_d. If k_d is much larger than the speed of water and ion transport, the flux of water and ions is negligible and the cell volume is almost conserved [Figs. 4(b) and 4(h)]. In contrast, if k_d is comparable to or even smaller than the speed of water and ion transport, the change of cell volume is significant and it will greatly influence the hydrostatic pressure difference, membrane tension, and contact angle (Fig. 4). Interestingly, cell volume increases (cell swelling) for convex cells [Fig. 4(b)], while it decreases (cell shrinkage) for concave cells [Fig. 4(h)] during detachment. Furthermore, under small k_d, the membrane reservoir can be activated for convex cells [Fig. 4(e)], since the cell volume (surface area) increases remarkably. Thus, there are some windings on the curves of ΔP, T_m, and θ_0. Depending on the cell volume change and k_d, the membrane tension T_m could increase or decrease and it is not monotonic [Figs. 4(e) and 4(k)]. The change of θ_0 [Figs. 4(f) and 4(l)] is inverse to the change of T_m due to the constraint of the Young-Dupré equation [Eq. (4)]. Therefore, θ_0 is not constant, which indicates the assumption of constant θ_0 used previously [20] might be invalid if cells are treated as open systems.

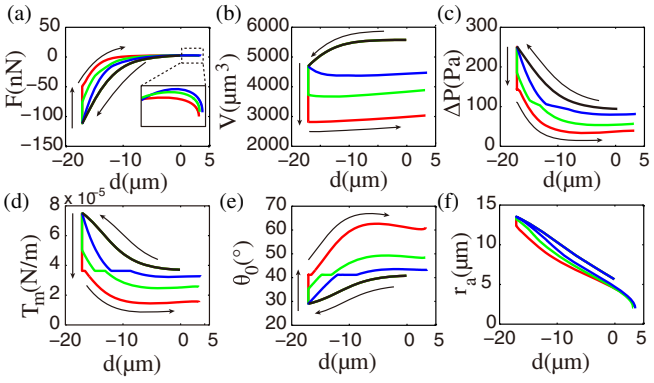

FIG. 5. The dynamic detachment of adhesive cells depends on loading history. The time evolution of the (a) external force, (b) cellular volume, (c) adhesion radius, (d) membrane tension, (e) contact angle, and (f) hydrostatic pressure difference of convex cells. For all the curves, $d_0 = 17$ μm, $k_c = k_d = 0.1$ μm/s, but the waiting time is different ($t_w = 0$, 400, and 800 s for the blue, green, and red curves). The black curves represent the loading stage.

For convex cells, the adhesion radius r_a first decreases steadily as d increases and then drops sharply when cell adhesion begins to rupture [Fig. 4(d)]. Conversely, for concave cells, r_a does not always decrease, but increases rapidly before the rupture [Fig. 4(j)]. This may be because convex cells rupture at the contact surfaces, while concave cells rupture at the necking equatorial section. These rupture forms are very similar to the rupture of liquid bridges [74].

Strikingly, our results for the dynamic spreading and detachment can quantitatively explain many existing experimental data (Fig. S13 [30]). Furthermore, we find the dynamic detachment of adherent cells also depends on loading history. To demonstrate it, we assume that the cell has already reached a steady state, and then we apply the loading-unloading process in Fig. 1(f) with various waiting times t_w. We find that the force, cell volume, contact angle, and other variables are very different (Fig. 5). This is because t_w is not long enough. Thus, the cell has not reached steady state before the cantilever is moved upward. In fact, the loading-unloading process in Fig. 1(f) is widely used in experiments [12–15], where the minimum t_w

needed to reach steady state can be affected by many factors, such as loading speed k_c, compression depth d_0, cell size, and cell type. Therefore, if t_w is not long enough, the mechanical response of cells in different experiments may not be comparable to each other.

In conclusion, we treated cells as open systems and studied how cell volume and pressure regulation influence the shape and dynamics of adherent cells. Our work showed that the mechanical response of living cells significantly depends on the complex interplay of cell volume change, loading rate, and loading history. Therefore, water and ion exchange with the environment is an essential factor that discriminates living cells from nonliving materials. Our findings may also have important implications for other biological processes accompanied by significant cell volume changes, such as mitotic cell rounding, cell deformation due to external forces, and haptotaxis or durotaxis induced by heterogeneous adhesion energy density or substrate stiffness.

This work was supported by the National Natural Science Foundation of China (Grants No. 11472271 and No. 11622222), the Thousand Young Talents Program of China, the Fundamental Research Funds for the Central Universities (Grant No. WK2480000001), and the Strategic Priority Research Program of the Chinese Academy of Sciences (Grant No. XDB22040403).

*Corresponding author.
jianghy@ustc.edu.cn

[1] H. F. Lodish, A. Berk, S. L. Zipursky, P. Matsudaira, D. Baltimore, J. Darnell *et al.*, Mol. Cell. Biol. **4** (2000).
[2] T. A. Springer *et al.*, Nature (London) **346**, 425 (1990).
[3] A. Elosegui-Artola, E. Bazellières, M. D. Allen *et al.*, Nat. Mater. **13**, 631 (2014).
[4] W. Engl, B. Arasi, L. Yap, J. Thiery, and V. Viasnoff, Nat. Cell Biol. **16**, 587 (2014).
[5] R. Mayor and S. Etienne-Manneville, Nat. Rev. Mol. Cell Biol. **17**, 97 (2016).
[6] E. Evans, D. Berk, and A. Leung, Biophys. J. **59**, 838 (1991).
[7] K. Prechtel, A. R. Bausch, V. Marchi-Artzner, M. Kantlehner, H. Kessler, and R. Merkel, Phys. Rev. Lett. **89**, 028101 (2002).
[8] B. Hogan, A. Babataheri, Y. Hwang, A. I. Barakat, and J. Husson, Biophys. J. **109**, 209 (2015).
[9] P.-H. Puech, K. Poole, D. Knebel, and D. J. Muller, Ultramicroscopy **106**, 637 (2006).
[10] S. Zou, H. Schonherr, and G. J. Vancso, J. Am. Chem. Soc. **127**, 11230 (2005).
[11] X. Liu, J. Q. Sun, M. H. Heggeness, M.-L. Yeh, and Z.-P. Luo, FEBS Lett. **563**, 23 (2004).
[12] O. Thoumine and J.-J. Meister, Eur. Biophys. J. **29**, 409 (2000).
[13] O. Thoumine and A. Ott, J. Cell Sci. **110**, 2109 (1997).
[14] N. Desprat, A. Richert, J. Simeon, and A. Asnacios, Biophys. J. **88**, 2224 (2005).
[15] D. Mitrossilis, J. Fouchard, D. Pereira, F. Postic, A. Richert, M. Saint-Jean, and A. Asnacios, Proc. Natl. Acad. Sci. U.S.A. **107**, 16518 (2010).
[16] O. Chaudhuri, S. H. Parekh, W. A. Lam, and D. A. Fletcher, Nat. Methods **6**, 383 (2009).
[17] V. T. Moy, Y. Jiao, T. Hillmann, H. Lehmann, and T. Sano, Biophys. J. **76**, 1632 (1999).
[18] Y.-S. Chu, S. Dufour, J. P. Thiery, E. Perez, and F. Pincet, Phys. Rev. Lett. **94**, 028102 (2005).
[19] M.-J. Colbert, A. Raegen, C. Fradin, and K. DalnokiVeress, Eur. Phys. J. E **30**, 117 (2009).
[20] F. Brochard-Wyart and P.-G. de Gennes, C.R. Phys. **4**, 281 (2003).
[21] S. Pierrat, F. Brochard-Wyart, and P. Nassoy, Biophys. J. **87**, 2855 (2004).
[22] M.-J. Colbert, F. Brochard-Wyart, C. Fradin, and K. Dalnoki-Veress, Biophys. J. **99**, 3555 (2010).
[23] H. Jiang and S. X. Sun, Biophys. J. **105**, 609 (2013).
[24] K. M. Stroka, H. Jiang, S.-H. Chen, Z. Tong, D. Wirtz, S. X. Sun, and K. Konstantopoulos, Cell **157**, 611 (2014).
[25] E. Zlotek-Zlotkiewicz, S. Monnier, G. Cappello, M. Le Berre, and M. Piel, J. Cell Sci. **211**, 765 (2015).
[26] J. Heo, F. Sachs, J. Wang, and S. Z. Hua, Cell. Physiol. Biochem. **30**, 395 (2012).
[27] I. Orhon *et al.*, Nat. Cell Biol. **18**, 657 (2016).
[28] M. P. Stewart, J. Helenius, Y. Toyoda, S. P. Ramanathan, D. J. Muller, and A. A. Hyman, Nature (London) **469**, 226 (2011).
[29] J. Irianto, J. Swift, R. P. Martins, G. D. McPhail, M. M. Knight, D. E. Discher, and D. A. Lee, Biophys. J. **104**, 759 (2013).
[30] See Supplemental Material at http://link.aps.org/supplemental/10.1103/PhysRevLett.118.208102, which includes Refs. [31–62], for more methods, discussions, figures, tables, and video files.
[31] M. Yoneda, J. Exp. Biol. **41**, 893 (1964).
[32] E. A. Evans, R. Skalak, and S. Weinbaum, *Mechanics and Thermodynamics of Biomembranes* (American Society of Mechanical Engineers, New York, 1980).
[33] E. Fischer-Friedrich, A. A. Hyman, F. Jülicher, D. J. Müller, and J. Helenius, Sci. Rep. **4**, 6213 (2015).
[34] S. Sukharev, B. Martinac, V. Y. Arshavsky, and C. Kung, Biophys. J. **65**, 177 (1993).
[35] D. Raucher and M. P. Sheetz, Biophys. J. **77**, 1992 (1999).
[36] L. Figard and A. M. Sokac, Bioarchitecture **4**, 39 (2014).
[37] B. Sinha, D. Koster, R. Ruez *et al.*, Cell **144**, 402 (2011).
[38] A. J. Kosmalska, L. Casares, A. Elosegui-Artola *et al.*, Nat. Commun., 7292 **6** (2015).
[39] R. Hochmuth and N. Mohandas, J. Biomech. **5**, 501 (1972).
[40] R. M. Hochmuth, N. Mohandas, and P. Blackshear Jr, Biophys. J. **13**, 747 (1973).
[41] E. A. Evans, Methods Enzymol. **173**, 3 (1989).
[42] L. Picas, F. Rico, and S. Scheuring, Biophys. J. **102**, L01 (2012).
[43] R. Rand, Biophys. J. **4**, 303 (1964).
[44] R. Hochmuth and R. Waugh, Annu. Rev. Physiol. **49**, 209 (1987).

[45] E. Evans and A. Yeung, Biophys. J. **56**, 151 (1989).
[46] A. R. Bausch, W. Möller, and E. Sackmann, Biophys. J. **76**, 573 (1999).
[47] E. J. Koay, A. C. Shieh, and K. A. Athanasiou, J. Biomech. Eng. **125**, 334 (2003).
[48] A. R. Bausch, F. Ziemann, A. A. Boulbitch, K. Jacobson, and E. Sackmann, Biophys. J. **75**, 2038 (1998).
[49] G. I. Bell *et al.*, Science **200**, 618 (1978).
[50] Y. Lin and L. B. Freund, Int. J. Solids Struct. **44**, 1927 (2007).
[51] J. Fouchard, C. Bimbard, N. Bufi, P. Durand-Smet, A. Proag, A. Richert, O. Cardoso, and A. Asnacios, Proc. Natl. Acad. Sci. U.S.A. **111**, 13075 (2014).
[52] H. Jiang, G. Huber, R. A. Pelcovits, and T. R. Powers, Phys. Rev. E **76**, 031908 (2007).
[53] H. Chen, T. Tang, and A. Amirfazli, Soft Matter **10**, 2503 (2014).
[54] T. R. Powers, G. Huber, and R. E. Goldstein, Phys. Rev. E **65**, 041901 (2002).
[55] M. P. Stewart, A. W. Hodel, A. Spielhofer, C. J. Cattin, D. J. Mller, and J. Helenius, Methods **60**, 186 (2013).
[56] K. D. Webster, W. P. Ng, and D. A. Fletcher, Biophys. J. **107**, 146 (2014).
[57] D. Mitrossilis, J. Fouchard, A. Guiroy, N. Desprat, N. Rodriguez, B. Fabry, and A. Asnacios, Proc. Natl. Acad. Sci. U.S.A. **106**, 18243 (2009).
[58] J. Y. Tinevez, U. Schulze, G. Salbreux, J. Roensch, J. F. Joanny, and E. Paluch, Proc. Natl. Acad. Sci. U.S.A. **106**, 18581 (2009).
[59] Mitra, K. I. Ubarretxena-Belandia, T. Taguchi, G. Warren, and D. M. Engelman, Proc. Natl. Acad. Sci. U.S.A. **101**, 4083 (2004).
[60] T. H. Hui, Z. L. Zhou, J. Qian, Y. Lin, A. H. W. Ngan, and H. Gao, Phys. Rev. Lett. **113**, 118101 (2014).
[61] E. H. Larsen, N. Møbjerg, and R. Nielsen, Comp. Biochm. Physiol., Part A, Mol. Integr. Physiol. **148**, 101 (2007).
[62] T. Erdmann and U. S. Schwarz, Phys. Rev. Lett. **92**, 108102 (2004).
[63] J. Dai and M. P. Sheetz, Biophys. J. **77**, 3363 (1999).
[64] A. Diz-Muñoz, D. A. Fletcher, and O. D. Weiner, Trends Cell Biol. **23**, 47 (2013).
[65] E. Fischer-Friedrich E, Y. Toyoda, C. J. Cattin, D. J. Müller, A. A. Hyman, and F. Jülicher, Biophys. J. **111**, 589 (2016).
[66] J. Tao and S. X. Sun, Biophys. J. **109**, 1541 (2015).
[67] L. Freund, Proc. Natl. Acad. Sci. U.S.A. **106**, 8818 (2009).
[68] A. Hategan, R. Law, S. Kahn, and D. E. Discher, Biophys. J. **85**: 2746 (2003).
[69] T. R. Powers, G. Huber, and R. E. Goldstein, Phys. Rev. E **65**, 041901 (2002).
[70] O. Pitois, P. Moucheront, and X. Chateau, Eur. Phys. J. B **23**, 79 (2001).
[71] O. Pitois, P. Moucheront, and X. Chateau, J. Colloid Interface Sci. **231**, 26 (2000).
[72] D. Rossetti, X. Pepin, and S. J. Simons, J. Colloid Interface Sci. **261**, 161 (2003).
[73] C. D. Willett, M. J. Adams, S. A. Johnson, and J. P. Seville, Langmuir **16**, 9396 (2000).
[74] A. Akbari and R. J. Hil, Soft Matter **12**, 6868 (2016).

Supplemental Material for "Shape and Dynamic of Adhesive Cell: Mechanical Response of Open Systems"

Yuehua Yang and Hongyuan Jiang*

CAS Key Laboratory of Mechanical Behavior and Design of Materials, Department of Modern Mechanics, University of Science and Technology of China, Hefei, Anhui, China

(Dated: April 27, 2017)

Contents

I. Model 1
A. Cell shape, effective surface area, and cellular volume 1
B. Cellular volume and pressure regulation 3
C. Constitutive laws of the cortical layer and membrane layer 4
1. The constitutive law of cortical layer 4
2. The reservoir model of membrane 4
3. The viscoelastic model of membrane 5
4. The contribution of the viscosities of cortex and membrane 7
D. The adhesion between cells and the two surfaces 8

II. Numerical Method 9

III. The Critical Condition of Tension-Induced Rupture 10

IV. Supplementary Results 12
A. Dynamic adhesion of cells (supplementary figures to the Fig. 3 in the main text) 12
B. The phase diagrams of cell shapes when cellular volume and pressure are constant. 13
C. Dynamic detachment of convex cells with negative initial F 14

V. The Ranges of Parameters 14

VI. The quantitative comparisons with experiments 15

References 16

I. MODEL

A. Cell shape, effective surface area, and cellular volume

We assume that the cell shape is cylindrically symmetric and can be described by (r(s), z(s)), where s is arc length (Fig. S1). Similar to previous works (Yoneda, 1964; Evans et al., 1980; Fischer-Friedrich et al., 2014), we deduce the two shape variables $r(s)$ and $z(s)$ mostly based on the force balance condition

$$2\pi\sigma hr\sin\theta = \Delta P\pi r^2 + F, \tag{S1}$$

where r is the cell radius, θ is the tangential angle of arc length, ΔP is the hydrostatic pressure differences, F is the external force (see Fig. S1). We assume that F is positive when cell is stretched, and F is negative when cell is compressed. To simplify the problem, the membrane and cortex can be modeled as a single layer with an equivalent stress σ. And h is the thickness of this layer, i.e., $h = h_m + h_c$, where h_m is the thickness of membrane layer and h_c is the thickness of cortical layer. From the force balance equation, we have

$$\sin\theta = Ar + B/r, \tag{S2}$$

*Corresponding author. jianghy@ustc.edu.cn

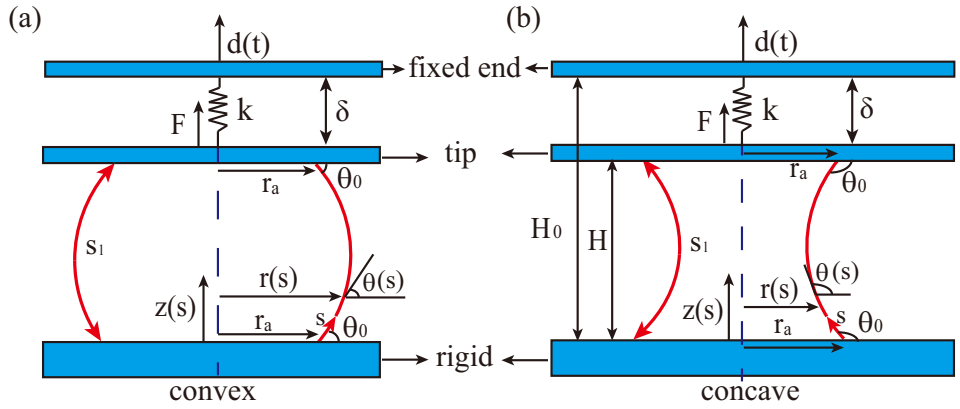

FIG. S1 Schematic of the convex cell (a) and concave cell (b) adhered symmetrically between an adhesive surface and a cantilever. The adhesive surface is rigid while the cantilever is flexible. And the cantilever is treated as a spring with a stiffness of k and zero rest length. Therefore the external force exerted on cell due to the deflection of cantilever is $F = k\delta$, where δ is the deflection of the cantilever. We describe the cell shape $(r(s), z(s))$ under the arc length coordinate, i.e., s with arrow in (a) and (b). $\theta(s)$ is the tangential angle. s_l is the total arc length of cell. The adhesion radius is r_a, and the contact angle is θ_0. H is the height of cell and H_0 is the separation of the adhesive surface and cantilever. $d(t)$ is the displacement of the fixed end of the cantilever.

where $A = \Delta P/(2\sigma h)$ and $B = F/(2\pi\sigma h)$.

Furthermore, the two shape variables $r(s)$ and $\theta(s)$ are related through the geometrical relation

$$\frac{dr}{ds} = \cos\theta. \tag{S3}$$

Substituting Eq. S2 into Eq. S3 yields

$$\frac{dr}{ds} = \pm\sqrt{1-(Ar+\frac{B}{r})^2}, \tag{S4}$$

where the positive and negative signs are taken for $\theta < 90^o$ and $\theta > 90^o$, respectively. Integrating Eq. S4, we can obtain

$$\pm 2As = -\arccos\frac{2A^2r^2-(1-2AB)}{\sqrt{1-4AB}} + C_0 \qquad \text{when} \quad 1-4AB > 0, \tag{S5}$$

where C_0 is an integration constant. C_0 is determined by enforcing $r(0) = r_a$, where r_a is the adhesion radius. On the lower boundary $\theta(0) = \theta_0$, where θ_0 is the contact angle. Therefore, on the boundary, we get $\sin\theta_0 = Ar_a + B/r_a$ based on Eq. S2. Notice that in this problem $1-4AB \geq 0$ is always true since $1-4AB = (1-2Ar_a)^2 + 4Ar_a(1-\sin\theta_0) \geq 0$. When the cell is cylindrical, $2Ar_a = 1$ and $\sin\theta_0 = 1$. Therefore, in this case $1-4AB = 0$ and the above solution in Eq. S5 does not exist. Thus, when cell is cylindrical we use another method to obtain the cell shape and we will discuss this in the section II.

From Eq. S5, we can obtain the cell radius $r(s)$ as

$$r^2 = \frac{1}{2A^2}\left[Q_1 + Q_2\cos(2As \mp \alpha_0)\right], \tag{S6}$$

where $Q_1 = 1-2AB$, $Q_2 = \sqrt{1-4AB}$, and $\alpha_0 = \arccos\left[(2A^2r_a^2 - Q_1)/Q_2\right]$. In contrary to Eq. S4, the positive and negative signs are taken for $\theta > 90^o$ and $\theta < 90^o$ in Eq. S6, respectively.

We can also obtain $z(s)$ by integrating $dz/ds = \sin\theta$ as

$$z(s) = \frac{1}{A\sqrt{2(Q_1+Q_2)}}\left[(Q_1+Q_2)E_2(As \pm \frac{\alpha_0}{2}, G) + 2ABE_1(As \pm \frac{\alpha_0}{2}, G)\right] + C_1, \tag{S7}$$

where C_1 is a constant and $G = 2Q_2/(Q_1+Q_2)$. $E_1(\theta, B)$ and $E_2(\theta, B)$ are the incomplete elliptic integrals of the

first and second kind, respectively.

$$E_1(\theta, m) = \int_0^\theta 1/\sqrt{1 - m\sin^2 x}dx,$$
$$E_2(\theta, m) = \int_0^\theta \sqrt{1 - m\sin^2 x}dx.$$

The boundary conditions for $z(s)$ are

$$z(0) = 0,$$
$$z(s_l) = H = 2r_0 + [d(t) - \delta],$$

where s_l is the total arclength, H is the cell height (Fig. S1), and r_0 is the initial cell radius, i.e., the radius of the spherical cells in suspension. $d(t)$ is the displacement of the fixed end of the cantilever, and δ is the deflection of the cantilever (Fig. S1). The arc length s_l is established by the condition $r(s_l) = r_a$. Therefore, from Eq. S6, we have $s_l = \alpha_0/A$ and $s_l = (\pi - \alpha_0)/A$ for convex cells and concave cells, respectively. From the boundary conditions, we can obtain the cell height H.

For convex cells,

$$H = \frac{\sqrt{2}}{A\sqrt{Q_1 + Q_2}}\left[(Q_1 + Q_2)E_2(\frac{\alpha_0}{2}, G) + 2ABE_1(\frac{\alpha_0}{2}, G)\right]. \tag{S8}$$

For concave cells,

$$H = \frac{\sqrt{2}}{A\sqrt{Q_1 + Q_2}}\left\{(Q_1 + Q_2)\left[E_2(\frac{\pi}{2}, G) - E_2(\frac{\alpha_0}{2}, G)\right] + 2AB\left[E_1(\frac{\pi}{2}, G) - E_1(\frac{\alpha_0}{2}, G)\right]\right\}. \tag{S9}$$

The effective surface area A_{eff} (the difference between the total surface area and the contact area) and cellular volume V can be calculated according to $A_{eff} = \int_0^{s_l} 2\pi r(s)ds$ and $V = \int_0^{s_l} \pi r(s)^2 \sin\theta(s)ds$.

For convex cells,

$$A_{eff} = \frac{2\sqrt{2}\pi}{A^2}\sqrt{Q_1 + Q_2}E_2(\frac{\alpha_0}{2}, G), \tag{S10}$$
$$V = \frac{\sqrt{2}\pi}{6A^3}\left\{2\sqrt{Q_1 + Q_2}(3AB + 2Q_1)E_2(\frac{\alpha_0}{2}, G) + (Q_2 - Q_1)\sqrt{Q_1 + Q_2}E_1(\frac{\alpha_0}{2}, G)\right.$$
$$\left. + Q_2\sin\alpha_0\sqrt{Q_1 + Q_2\cos\alpha_0}\right\}. \tag{S11}$$

For concave cells,

$$A_{eff} = \frac{2\sqrt{2}\pi}{A^2}\sqrt{Q_1 + Q_2}\left[E_2(\frac{\pi}{2}, G) - E_2(\frac{\alpha_0}{2}, G)\right], \tag{S12}$$
$$V = \frac{\sqrt{2}\pi}{6A^3}\left\{2\sqrt{Q_1 + Q_2}(3AB + 2Q_1)\left[E_2(\frac{\pi}{2}, G) - E_2(\frac{\alpha_0}{2}, G)\right]\right.$$
$$\left. + (Q_2 - Q_1)\sqrt{Q_1 + Q_2}\left[E_1(\frac{\pi}{2}, G) - E_1(\frac{\alpha_0}{2}, G)\right] - Q_2\sin\alpha_0\sqrt{Q_1 + Q_2\cos\alpha_0}\right\}. \tag{S13}$$

B. Cellular volume and pressure regulation

The time evolution of cellular volume V and ion number n due to the water and ions transport are given as

$$\frac{dV}{dt} = -L_pA_{eff}(\Delta P - \Delta\Pi), \tag{S14}$$
$$\frac{dn}{dt} = A_{eff}(J_{out} + J_{in}). \tag{S15}$$

where A_{eff} is the effective surface area without considering the adhesion area since there are no ion and water transport across the contact surfaces. L_p is the rate of membrane permeability to water. $\Delta P = P_{in} - P_{out}$ and

$\Delta\Pi = \Pi_{in} - \Pi_{out}$ are hydrostatic and osmotic pressure differences, respectively. The osmotic pressure inside the cell can be determined by the Van't Hoff equation $\Pi = cRT$, where $c = n/V$ is the concentration of solutes, R is the gas constant, and T is the absolute temperature. For the time evolution of ion number, J_{out} is the ion efflux due to the opening of mechanosensitive channels, and J_{in} is the influx of ions through active ion pumps.

For a mechanosensitive channel, the opening probability P_{open} is a Boltzmann function of the surface tension (Sukharev et al., 1993). After approximating the Boltzmann function by a piecewise linear function (Jiang and Sun, 2013), we have

$$J_{out} = \begin{cases} 0 & \text{if} \quad \sigma < \sigma_c, \\ -\beta(\sigma - \sigma_c)\Delta\Pi & \text{if} \quad \sigma_c \leq \sigma \leq \sigma_s, \\ -\beta(\sigma_s - \sigma_c)\Delta\Pi & \text{if} \quad \sigma > \sigma_s. \end{cases} \tag{S16}$$

where β is the rate constant of efflux, σ_c and σ_s are the threshold stress (below which no mechanosensitive channel is open) and saturating stress (above which all mechanosensitive channels are open) of the mechanosensitive channels, respectively.

In addition to mechanosensitive channels, ion transporters actively pump ions against concentration gradients. In order to overcome the energy barrier from the ion concentration gradient, ion transporters utilize energy from ATP hydrolysis. We denote ΔG_a as the free energy input during the pumping action. The free energy change during the pumping action is $\Delta G = RT\log(c_{in}/c_{out}) - \Delta G_a$, where c_{in} and c_{out} are the ion concentration inside and outside the cell, respectively. The ion flux across transporters can be modeled as $J_{in} = -\gamma'\Delta G$, where γ' is a constant. By assuming $c_{in} - c_{out} \ll c_{in}$, ΔG can be linearized as $\Delta G \approx RT(c_{in} - c_{out})/c_{out} - \Delta G_a = RT(\Pi_{in} - \Pi_{out})/\Pi_{out} - \Delta G_a$. Therefore, the influx of ions can be described by (Jiang and Sun, 2013)

$$J_{in} = \gamma(\Delta\Pi_c - \Delta\Pi) \tag{S17}$$

where γ is a constant and $\Delta\Pi_c = \Pi_{out}[exp(\Delta G_a/RT) - 1]$ is the critical osmotic pressure difference related to osmotic pressure outside the cells. The critical osmotic pressure difference is the osmotic pressure difference above which the energy input from ATP is insufficient for ion transporters to pump ions against the concentration gradient. The free energy from a mole ATP is $\Delta G_a \approx 30kJ$, and the osmotic pressure of the growth medium is $\Pi_{out} = 0.5MPa$, which yields a critical osmotic pressure difference $\Delta\Pi_c \approx 30GPa$.

C. Constitutive laws of the cortical layer and membrane layer

The surface tension of the cell, T_s, is the combined result of cortical tension, T_{cortex}, and membrane tension, T_m, i.e., $T_s = T_{cortex} + T_m$ (Dai and Sheetz, 1999; Diz-Muñoz et al., 2013). The cortical tension is related to the cortical stress as $T_{cortex} = \sigma_{cortex}h_c$, where h_c is the thickness of cortical layer and σ_{cortex} is the cortical stress. The membrane tension is $T_m = \sigma_m h_m$, where h_m is the thickness of membrane and σ_m is the membrane stress. We can define an equivalent surface stress σ in the combined layer by $\sigma h = T_s$, where $h = h_m + h_c$. Therefore, the surface stress can be determined by $\sigma(h_m + h_c) = \sigma_{cortex}h_c + \sigma_m h_m$.

1. The constitutive law of cortical layer

The cortical layer can be modeled as a fluid-like layer with an active stress. Thus, the constitutive law of the cortical layer is given as

$$\sigma_{cortex} = \eta\dot{\varepsilon}_A + \sigma_a, \tag{S18}$$

where η is the viscosity of cortical layer, $\dot{\varepsilon}_A$ is the strain rate of cellular surface area, and σ_a is the active stress of cortical layer due to the contraction of myosin motors.

2. The reservoir model of membrane

It is well known that the presence of membrane reservoirs can buffer the increase of membrane tension during the changing of cellular shape (Raucher and Sheetz, 1999; Figard and Sokac, 2014; Sinha et al., 2011). In the tether experiment carried out by Raucher et al with optical tweezers (Raucher and Sheetz, 1999), it has been found that the tether force shows three phases, i.e., an initial phase (the tether force increases with the tether length), an elongation

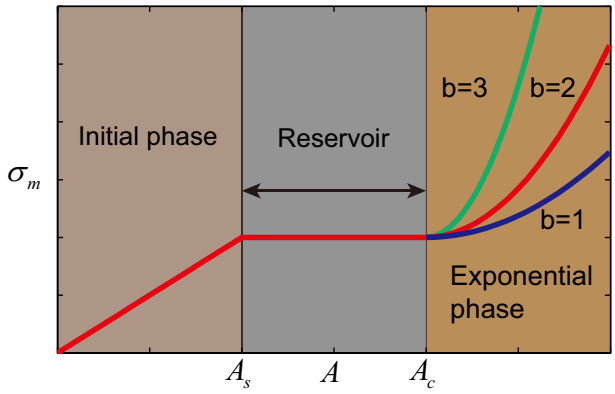

FIG. S2 The constitutive law of cell membrane after considering the membrane reservoirs. Membrane stress increases linearly with cellular surface area in the initial phase. And the membrane stress is independent on cellular surface area in the reservoir phase. In the third phase, the membrane stress increases exponentially with surface area, i.e., $\sigma_m \propto E_n[e^{b(A-A_c)/A_0}-1]$, where b and E_n are constant. A_s is the critical surface area where the reservoir is activated, and A_c is the critical surface area when the reservoir is depleted.

phase (the tether force is constant, buffered by the membrane reservoir) and an exponential phase (the tether force increases exponentially with the tether length).

The tether force is an indicator of the effective membrane tension. Thus, according to this experimental result, we model the membrane stress σ_m as a function of cellular surface area A as (see Fig. S2)

$$\sigma_m = \begin{cases} E_m(A-A_0)/A_0 & \text{if} \quad A < A_s, \\ E_m(A_s-A_0)/A_0 & \text{if} \quad A_s \le A \le A_c, \\ E_m(A_s-A_0)/A_0 + E_n[e^{b(A-A_c)/A_0}-1] & \text{if} \quad A > A_c, \end{cases} \tag{S19}$$

where E_m is the elastic modulus of membrane in the initial phase, A is the deformed surface area, A_0 is the reference surface area, A_s is the critical surface area where the reservoir is activated, and A_c is the critical surface area where the reservoir is depleted. Therefore, A_c/A_s-1 is proportional to the size of membrane reservoir, and the reservoir size found in experiment is in the range of $1\% \sim 30\%$ (Figard and Sokac, 2014; Sinha et al., 2011; Kosmalska et al., 2015). After the depletion of membrane reservoir, we assume the membrane stress, σ_m, is an exponential function of cellular surface area, i.e., $\sigma_m \propto E_n[e^{b(A-A_c)/A_0}-1]$, where b and E_n are constant. When $A_c = A_s$, $E_m = bE_n$, and $(A-A_c)/A_0$ is small, this constitutive law of the membrane reduces to an elastic constitutive law, i.e., $\sigma_m = E_m(A-A_0)/A_0$. For simplicity, we assume $bE_n = E_m$ in our simulations. Substituting Eq. S18 and Eq. S19 into $h\sigma = h_m\sigma_m + h_c\sigma_{cortex}$, we can obtain the constitutive law of surface stress σ.

As shown in Fig. S3, for different b and reservoir size A_c/A_s, the qualitative results of the phase diagram of the dynamic adhesion are the same. These results indicate that the adhesion behaviors, studied in this work, are not sensitive to the constitutive law of membrane.

3. The viscoelastic model of membrane

We can also use a viscoelastic model for the membrane. In this case, the general viscoelastic constitutive law of membrane layer is

$$\sigma_m + a_1\dot{\sigma}_m = b_0\varepsilon_A + b_1\dot{\varepsilon}_A, \tag{S20}$$

where $\dot{\sigma}_m$ is the stress rate of membrane layer, ε_A is the area strain, a_1, b_0 and b_1 are constants. This viscoelastic constitutive law can be reduced to Kelvin-Voigt model when a_1=0, Maxwell model when b_0=0, three-element Kelvin model, and three-element Maxwell model.

Based on the constitutive laws of cortical layer and membrane, i.e., Eq. S18 and Eq. S20, we obtain

$$h\sigma + a_1h\dot{\sigma} \;=\; h_c(\eta\dot{\varepsilon}_A + \sigma_a) + a_1h_c\eta\ddot{\varepsilon}_A + h_m(b_0\varepsilon_A + b_1\dot{\varepsilon}_A). \tag{S21}$$

When we use the three-element Maxwell model to describe the deformation of membrane (Fig. S4), the constitutive law of membrane Eq. S20 becomes

$$\sigma_m + \eta_m/E_1\dot{\sigma}_m = E_0\varepsilon_A + (E_1+E_0)\eta_m/E_1\dot{\varepsilon}_A, \tag{S22}$$

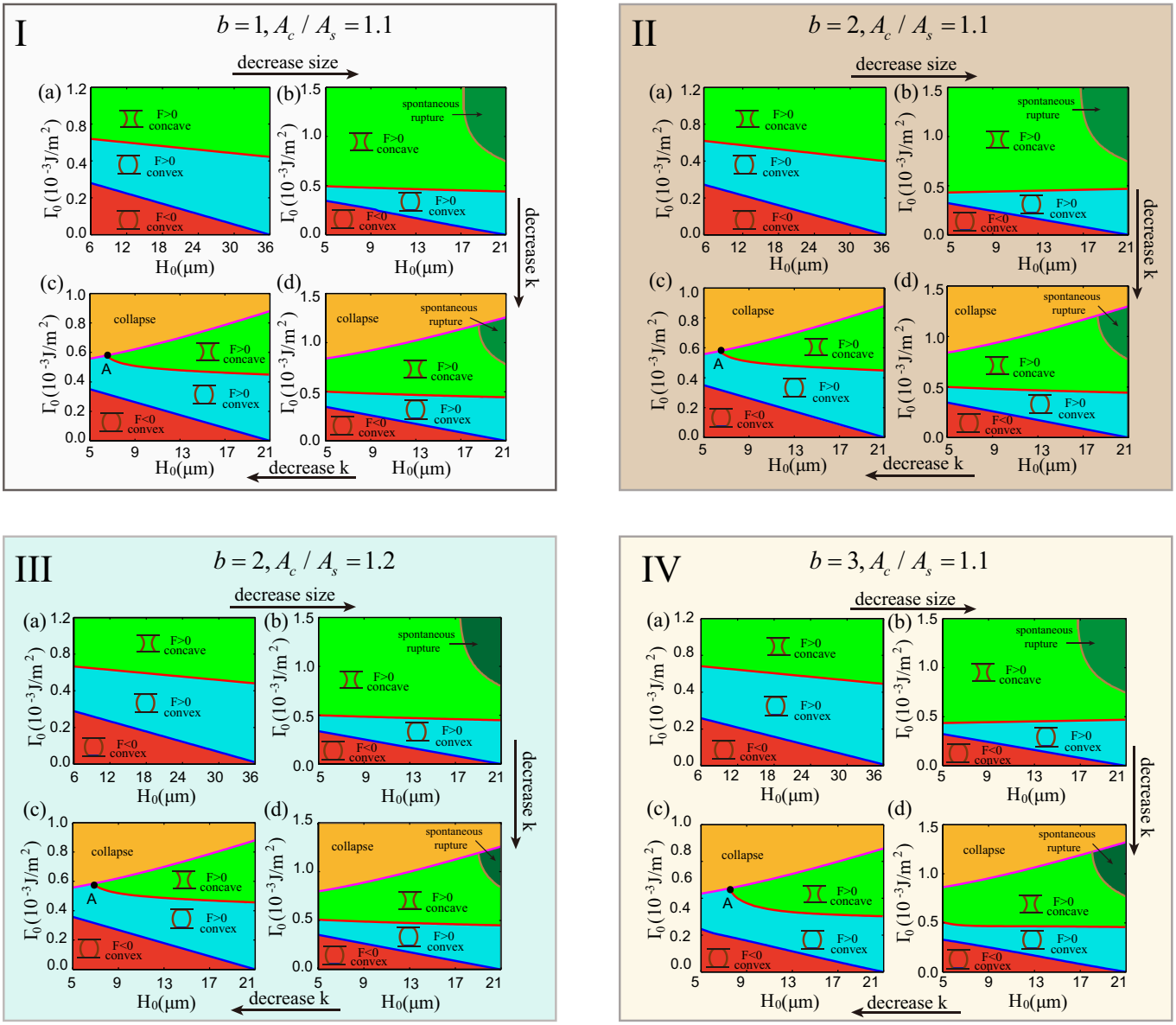

FIG. S3 The phase diagrams of cell shapes for various stiffness of cantilever k and cell size r_0, when we consider the effect of membrane reservoir for different b and reservoir size A_c/A_s. (I) $b = 1$ and $A_c/A_s = 1.1$; (II) $b = 2$ and $A_c/A_s = 1.1$; (III) $b = 2$ and $A_c/A_s = 1.2$; (IV) $b = 3$ and $A_c/A_s = 1.1$. In each subfigure, (a) $r_0 = 18\mu m$, $k = 0.5N/m$; (b) $r_0 = 10.5\mu m$, $k = 0.5N/m$; (c) $r_0 = 10.5\mu m$, $k = 0.005N/m$; (d) $r_0 = 10.5\mu m$, $k = 0.01N/m$. We can find that for different constitutive laws, the qualitative results of dynamic adhesion are the same.

where E_1 and E_0 are the two spring constants of the three-element Maxwell model, and η_m is the viscosity of membrane (Fig. S4).

Therefore the constitutive law of surface stress Eq. S21 becomes

$$h\sigma + \eta_m/E_1\dot{\sigma}h = h_c(\eta\dot{\varepsilon}_A + \sigma_a) + h_c\eta\eta_m/E_1\ddot{\varepsilon}_A + h_m[E_0\varepsilon_A + (E_1 + E_0)\eta_m/E_1\dot{\varepsilon}_A]. \tag{S23}$$

The elastic modulus of membrane ranges from 10^4 Pa to 10^7 Pa (Hochmuth and Mohandas, 1972; Hochmuth et al., 1973; Evans, 1989; Picas et al., 2012). Therefore, we take $E_0 = 100\ kPa$ and $E_1 = 40\ kPa$ in our simulation. It has been shown that the relaxation time of membrane is on the order of 0.1 second (Evans, 1989; Rand, 1964; Hochmuth and Waugh, 1987), which gives the ratio of the membrane viscosity, η_m, to the elastic modulus E_1. Thus, we take $\eta_m = 4000\ Pa \cdot s$. The viscosity of cortical layer measured in experiments is about $10^2 \sim 10^3 Pa \cdot s$ (Evans and Yeung, 1989; Bausch et al., 1999; Koay et al., 2003; Bausch et al., 1998), so we take $\eta = 5000 Pa \cdot s$.

We find that the qualitative results of the viscoelastic model are the same with the results of the reservoir model

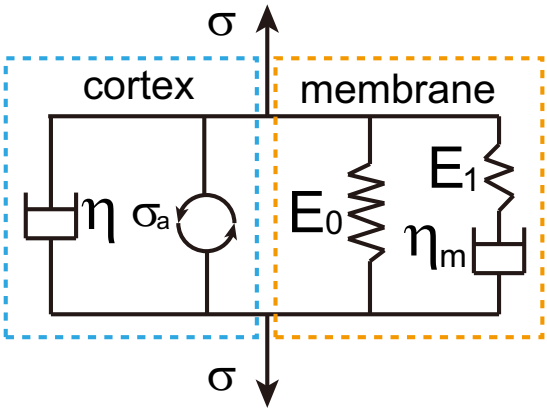

FIG. S4 The fluid-like cortical layer model with active contraction and the three-element Maxwell model of cell membrane. The cell surface stress σ is the combined effect of membrane stress and cortical stress since these two layers are connected in parallel. η is the viscosity of cortical layer and σ_a is the active stress of cortex. E_1 and E_0 are the two spring constants of the three-element Maxwell model, and η_m is the viscosity of membrane.

(compare Fig. S5(I) with Fig. S3). Therefore, we will take the reservoir model, Eq. S19, to describe the deformation of membrane in our main text.

4. The contribution of the viscosities of cortex and membrane

To investigate the roles of the viscosities of cortex and membrane in cell responses, we first study the dynamic adhesion of cell when we neglect the contribution of the viscous terms in Eq. S21 and Eq. S23. In this case, the constitutive law of surface stress reduces to an elastic constitutive law

$$h\sigma = h_m E_m (A/A_0 - 1) + \sigma_a h_c, \tag{S24}$$

where E_m is the Young's modulus of membrane layer, A and A_0 are the deformed and reference cellular surface areas, respectively. After takeing an elastic constitutive law for the surface stress (Eq S24), the qualitative results of the

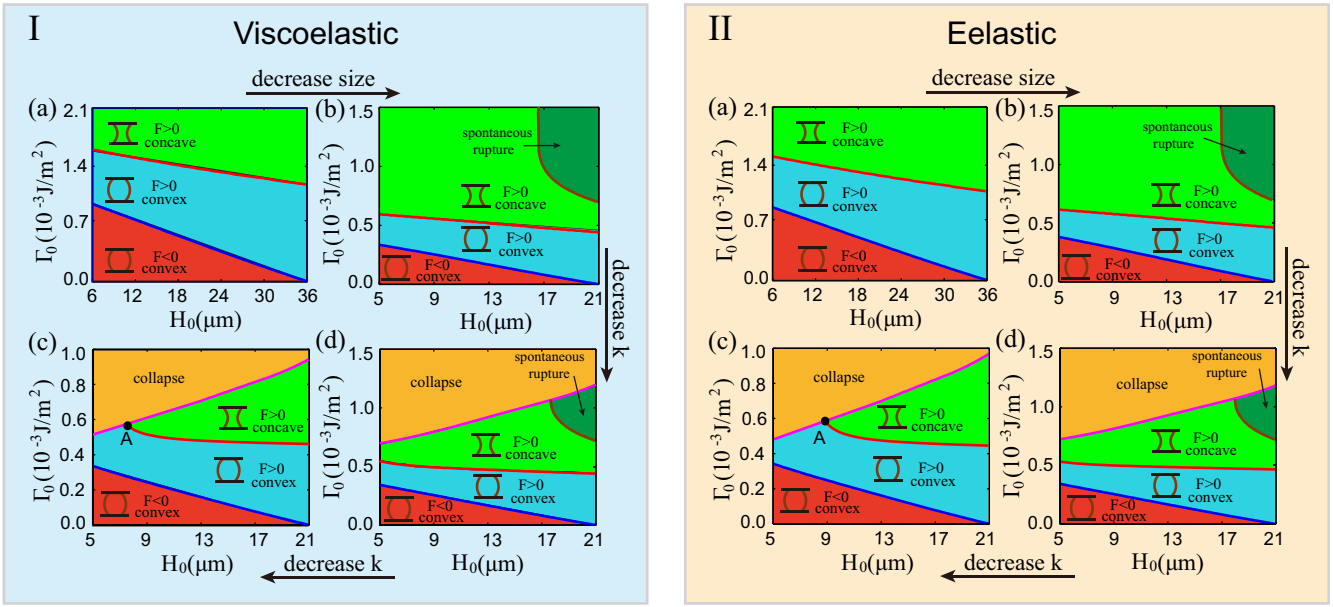

FIG. S5 The phase diagrams of cell shapes for various stiffness of cantilever k and cell size r_0 when we take a viscoelastic (I, η=5000 $Pa \cdot s$, η_m=4000 $Pa \cdot s$) or an elastic (II, η=0 $Pa \cdot s$, η_m=0 $Pa \cdot s$) constitutive law of cortex and membrane. (a) $r_0 = 18\mu m$, $k = 0.5N/m$; (b) $r_0 = 10.5\mu m$, $k = 0.5N/m$; (c) $r_0 = 10.5\mu m$, $k = 0.005N/m$; (d) $r_0 = 10.5\mu m$, $k = 0.01N/m$.

phase diagram of the dynamic adhesion behaviors of cell are the same with the results of the viscoelastic model (Fig. S5 I and II).

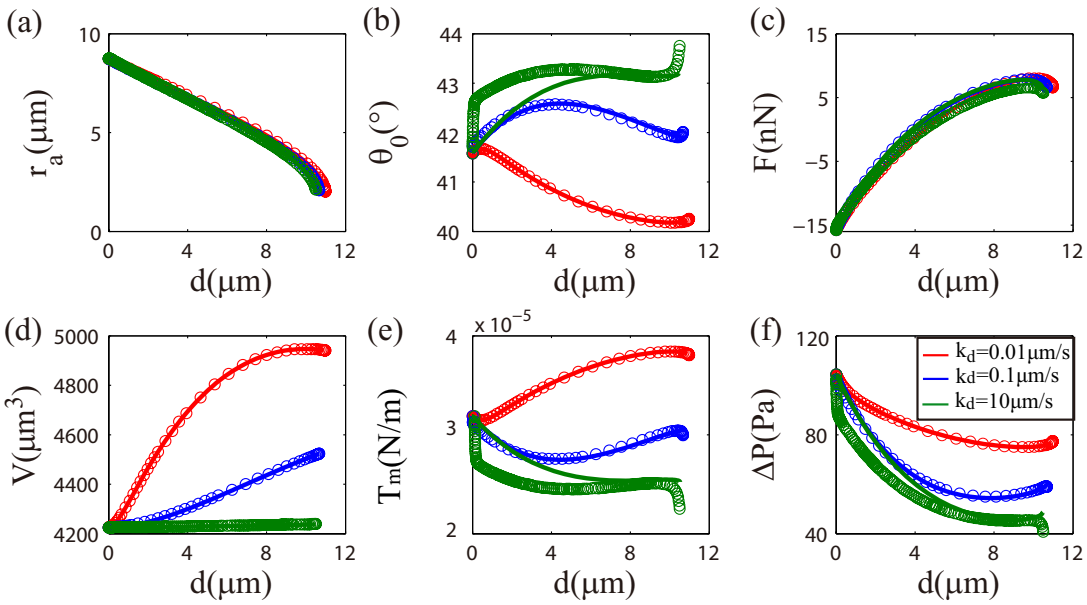

FIG. S6 The detachment of convex cells, when the viscosities of cortical layer and membrane layer are zero (solid curves) or nonzero (circles, $\eta = 5000 Pa \cdot s$ and η_m=4000 $Pa \cdot s$). (a) The adhesion radius, (b) contact angle, (c) external force, (d) cellular volume, (e) membrane tension, and (f) the hydrostatic pressure difference. The viscous properties of the cortical layer and membrane layer only slightly affect the response of cells when $k_d > 10 \mu m/s$.

To what extent do the viscosities of cortex and membrane contribute to the responses of cell? As shown in Fig. S6, we compare the detachment results of the viscoelastic constitutive law ($\eta = 5000 Pa \cdot s$ and η_m=4000 $Pa \cdot s$) with the results of an elastic constitutive law ($\eta = 0$ and $\eta_m = 0$). The loading speed k_d used in our simulation is $0.01 \sim 10$ $\mu m/s$ since the stretch speed used in experiment is $0.1 \mu m/s \sim 10$ $\mu m/s$ (Thoumine and Meister, 2000; Colbert et al., 2009, 2010; Chu et al., 2005). We find that the contributions of the viscosities of the fluid-like cortical layer and membrane to the detachment of cells are significant under high stretch speed.

D. The adhesion between cells and the two surfaces

The adhesion between cells and the two surfaces can be described by the Young–Dupré equation as

$$\Gamma = \sigma h(1 - \cos\theta_0), \tag{S25}$$

where Γ is the adhesion energy density and θ_0 is the contact angle.

The rate equation of the ligand-receptor bonds density ρ_{lr} is given by (Bell et al., 1978; Lin and Freund, 2007)

$$\frac{d\rho_{lr}}{dt} = k_{on}\rho_l\rho_r - k_{off}\rho_{lr}, \tag{S26}$$

where ρ_l is the ligand density and ρ_r is the receptor density. k_{on} and k_{off} are the association and dissociation rates, respectively. Here we assume that there are reservoirs for ligand and receptor so that the ligand density ρ_l and receptor density ρ_r are constants. We further assume that the association rate k_{on} is force independent, while the dissociation rate k_{off} increases exponentially with the external force f on the ligand-receptor bond according to Bell's model (Bell et al., 1978; Lin and Freund, 2007)

$$k_{off} = k^0_{off} exp(af/k_BT), \tag{S27}$$

where k^0_{off} is the dissociation rate of ligand-receptor pairs when $f = 0$, a is the characteristic length of the bond deformation, k_B is the Boltzmann's constant, and T is the absolute temperature. We assume that the traction force F is equally shared by all the bonds in the adhesion area, i.e., $f = F/(\pi r_a^2 \rho_{lr})$, where r_a is the adhesion radius.

When the bonds are unloaded, on equilibrium we have $k_{on}\rho_l\rho_r - k^0_{off}\rho^0_{lr} = 0$, where ρ^0_{lr} is the equilibrium ligand-receptor pair density when $F = 0$. So the rate equation reduces to

$$\frac{d\rho_{lr}}{dt} = k^0_{off}\rho^0_{lr} - k_{off}\rho_{lr} \tag{S28}$$

Substituting Eq. S27 to Eq. S28, the rate equation becomes

$$\frac{d\rho_{lr}}{dt} = k^0_{off}\rho^0_{lr}\left[1 - \frac{\rho_{lr}}{\rho^0_{lr}} exp(\frac{af}{k_BT})\right], \tag{S29}$$

If we assume the rupture energy of single bond is V_e, then the adhesion energy density is $\Gamma = V_e\rho_{lr}$. Thus the time evolution of Γ is

$$\frac{d\Gamma}{dt} = V_e\frac{d\rho_{lr}}{dt} = k^0_{off}\Gamma_0\left[1 - \frac{\Gamma}{\Gamma_0} exp(\frac{aFV_e}{k_BT\Gamma\pi r_a^2})\right]. \tag{S30}$$

where $\Gamma_0 = V_e\rho^0_{lr}$ is the equilibrium adhesion energy density when $F = 0$.

It should be noted that if we assume that only the ligand-receptor bonds adjacent to the periphery of adhesion region are being stretched, we only need to modify $f = F/(\pi r_a^2\rho_{lr})$ to $f = F/(\pi r_a d\rho_{lr})$, where d is the width of the annular region. We find the results of these two cases are qualitatively the same.

Recent experiment demonstrated that the spread radius r_s is bigger than the cell body contact radius r_a due to the existence of lamellipodia (Fouchard et al., 2014). In our model, to simplify the problem we have neglected the lamella and assumed the spread area r_s is equal to the cell body contact radius r_a. If we consider the difference between r_s and r_a, we can simply modify $f = F/(\pi r_a^2\rho_{lr})$ to $f = F/(\pi r_s^2\rho_{lr})$. Therefore, we can determine the effective adhesion energy density from Eq. S30. It should be noted that if F is bigger than a critical value $F_c = k_BT\pi r_a^2\Gamma_0/(eaV_e)$, there is no steady solution in Eq. S30. However, we find that F is much smaller then F_c for the parameters used in our simulation.

II. NUMERICAL METHOD

The analytical solution we obtained above has some limitations. It's only suitable for simple cell shapes with monotonically changing θ. Furthermore, the analytical solution in Eq. S6 will break down for cylindrical cells since $\theta = \pi/2$ and Eq. S3 reduces to $dr/ds = 0$ in this case. Consequently, it's very necessary to develop a method to solve for arbitrary cell shapes. Here, we obtain the cell shape by numerically solving a boundary value problem following our previous work (Jiang et al., 2007).

At any given time t, the cell shape r(s) and z(s) can be described by the following ordinary differential equations (Chen et al., 2014)

$$\frac{dr}{ds} = \cos\theta, \tag{S31}$$

$$\frac{dz}{ds} = \sin\theta. \tag{S32}$$

$$\frac{d\theta}{ds} = \frac{\Delta P}{\sigma h} - \frac{\sin\theta}{r} = \frac{B_1}{r_a} - \frac{\sin\theta}{r}, \tag{S33}$$

where $B_1 = \Delta P r_a/(\sigma h)$ is an unknown dimensionless variable. Eq. S31 and Eq. S32 are the geometric relations while Eq. S33 is deduced from Young–Laplace equation.

It is convenient to regard the effective surface area as a function of s. We define $A_s(s)$ as the effective surface area swiped by the arclength s, similarly, we can define $V_s(s)$. Thus, $A_s(s)$ and $V_s(s)$ obey the following differential equations

$$\frac{dA_s}{ds} = 2\pi r, \tag{S34}$$

$$\frac{dV_s}{ds} = \pi r^2\sin\theta. \tag{S35}$$

The corresponding boundary conditions are $A_s(0) = 0$, $A_s(s_l) = A_{eff}$, $V_s(0) = 0$, and $V_s(s_l) = V$, where A_{eff} and V are the effective surface area and the cellular volume of the whole cell, respectively. Other boundary conditions

include $r(0) = r_a$, $r(s_l) = r_a$, $\theta(0) = \theta_0$, $\theta(s_l) = \pi - \theta_0$, $z(0) = 0$, and $z(s_l) = 2r_0 + (d - \delta)$. Here r_a is the adhesion radius, θ_0 is the contact angle, and $2r_0 + (d - \delta)$ is the cell height as we discussed in the above sections.

The arclength s_l is still unknown and must be solved for along with the cell shape. To determine s_l, we introduce a new variable x with $s = s_l x$ and $x \in [0, 1]$ to reparametrize the problem (Jiang et al., 2007). Thus, the boundary conditions at $s = s_l$ transform to the boundary conditions at $x = 1$. And the differential equations are also modified to

$$\frac{dr}{dx} = s_l \cos\theta, \tag{S36}$$

$$\frac{dz}{dx} = s_l \sin\theta, \tag{S37}$$

$$\frac{d\theta}{dx} = s_l \frac{B_1}{r_0} - s_l \frac{\sin\theta}{r}, \tag{S38}$$

$$\frac{dA}{dx} = 2\pi s_l r, \tag{S39}$$

$$\frac{dV}{dx} = \pi r^2 s_l \sin\theta, \tag{S40}$$

$$\frac{ds_l}{dx} = 0. \tag{S41}$$

In our numerical approach, we treat these differential equations as a two-point boundary value problem, and we use the MATLAB function **bvp4c** to solve this boundary value problem.

III. THE CRITICAL CONDITION OF TENSION-INDUCED RUPTURE

Since cell would spontaneously rupture under strong adhesion, it is necessary to obtain the critical condition for spontaneous rupture. The analytical relation between the equilibrium cell shape and mechanical parameters, such as surface tension T_s, hydrostatic pressure difference ΔP, and the stiffness of cantilever k, at the time of rupture can be determined by the following analytic model.

The free energy of the system is

$$\begin{aligned} G &= \int \sigma h dS - \int \Delta P dV, \\ &= \int \sigma h 2\pi r(z)\sqrt{1 + (dr/dz)^2} dz - \int \Delta P \pi r(z)^2 dz \end{aligned} \tag{S42}$$

where σh is the surface tension, and ΔP is the hydrostatic pressure differences. By non-dimensionalizing the free energy with $\pi\sigma h r_0^2$, the free energy then becomes

$$\tilde{G} = \frac{G}{\pi\sigma h r_0^2} = \int 2\tilde{r}\sqrt{1 + (d\tilde{r}/d\tilde{z})^2} d\tilde{z} - \int B_2 \tilde{r}^2 d\tilde{z}, \tag{S43}$$

where $\tilde{r} = r/r_0$, $\tilde{z} = z/r_0$, $B_2 = \Delta P r_0/(\sigma h)$ are dimensionless variables, and r_0 is the initial cell size (the radius of the spherical cell in suspension). We minimize the energy $\tilde{G}$ by taking the first variational derivative with respect to $\tilde{z}$ and obtain the following Euler-Lagrange equation

$$\frac{2\tilde{r}}{\sqrt{1 + (d\tilde{r}/d\tilde{z})^2}} - B_2 \tilde{r}^2 = A_2, \tag{S44}$$

where $A_2 = F/(\pi\sigma h r_0)$ is the conserved quantity of the system. When $\Delta P = 0$ (i.e. $B_2 = 0$), this Euler-Lagrange equation reduces to the shape equation of a catenoid (Powers et al., 2002). Integrating Eq. S44 yields the cell shape

$$\tilde{z} = \begin{cases} F_1(\tilde{r}) - F_1(\tilde{r}_a) + \tilde{H} & \text{when} \quad \theta < \pi/2, \\ F_1(\tilde{r}_a) - F_1(\tilde{r}) & \text{when} \quad \theta \geq \pi/2, \end{cases} \tag{S45}$$

where $\tilde{r_a}$ and $\tilde{H}$ are the dimensionless adhesion radius and cell height, respectively. The detailed expression of $F_1(r)$

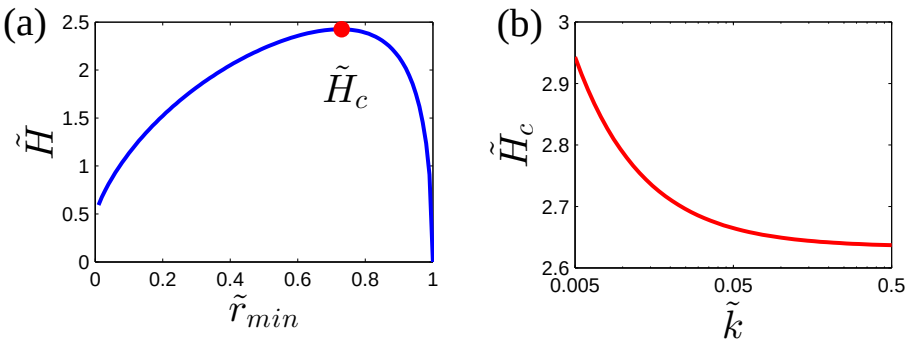

FIG. S7 (a) Cell height $\tilde{H}$ vs minimum neck radius $\tilde{r}_{min}$. There is critical cell height $\tilde{H}_c$ beyond which on solution exists. (b) The critical cell height $\tilde{H}_c$ decreases with an increase in the stiffness of cantilever $\tilde{k}$.

is

$$F_1(r) = \frac{\sqrt{1+B_2^2r^2/P_1}\sqrt{P_2-B_2^2r^2}}{B_2^2\sqrt{4r^2-(A_2+B_2r^2)^2}}\left[P_1E_2\left[\phi(r),-P_2/P_1\right]+2\sqrt{1-A_2B_2}E_1\left[\phi(r),-P_2/P_1\right]\right], \tag{S46}$$

where $P_1 = (1-\sqrt{1-A_2B_2})^2$, $P_2 = (1+\sqrt{1-A_2B_2})^2$, and $\phi(r) = \arcsin(B_2r/(1+\sqrt{1-A_2B_2}))$. $E_1(\theta,m)$ and $E_2(\theta,m)$ are the incomplete elliptic integrals of the first and second kind, respectively. For given surface tension σh, hydrostatic pressure difference ΔP, cell height H and adhesion radius r_a, the equilibrium cell shape is analytically determined by Eq. S45.

The separation between the adhesive surface and cantilever, H_0, is related to the cell height, H, through $H_0 = H + F/k$, where F is the external force applied by the cantilever and k is the stiffness of the cantilever. After non-dimensionalization, we have

$$\tilde{H}_0 = \tilde{H} + A_2/\tilde{k} = 2F_1(\tilde{r}_a) - 2F_1(\tilde{r}_{min}) + A_2/\tilde{k} \tag{S47}$$

where $\tilde{r}_{min}$ is the minimum cell radius where $d\tilde{r}/d\tilde{z} = 0$ at the equatorial plane ($\theta = \pi/2$), and $\tilde{k} = k/(\pi\sigma h)$ is the dimensionless stiffness of the cantilever. Notice that, the adherent cell only ruptures at concave shape, so the cell radius at $d\tilde{r}/d\tilde{z} = 0$ is minimum. Since there is a maximum in the curve of $\tilde{H}$ (marked by a red dot in Fig. S7(a)), there is a critical cell height $\tilde{H}_c$ beyond which no solution exists. It indicates that for the cell height bigger than this critical height, there is no corresponding neck radius r_{min}, i.e., no corresponding equilibrium cell shape exists.

The critical condition for the tension-induced rupture is

$$\begin{aligned}\frac{d\tilde{H}}{dA_2} &= \frac{2\tilde{r}_aA_2B_2(2-A_2B_2-B_2^2\tilde{r}_a^2)}{A_2(A_2B_2-1)H_1(\tilde{r}_a)H_2(\tilde{r}_a)} - \frac{2A_2B_2\tilde{r}_{min}(2-2B_2\tilde{r}_{min})}{A_2(A_2B_2-1)H_1(\tilde{r}_{min})H_2(\tilde{r}_{min})} + \\ &\frac{2\sqrt{P_1}\sqrt{4\tilde{r}_a^2-(A_2+B_2\tilde{r}_a)^2}}{A_2(A_2B_2-1)H_1(\tilde{r}_a)H_2(\tilde{r}_a)}\left[P_1E_2\left[\phi(\tilde{r}_a),-P_2/P_1\right]-2\sqrt{1-A_2B_2}E_1\left[\phi(\tilde{r}_a),-P_2/P_1\right]\right] = 0,\end{aligned} \tag{S48}$$

where $H_1(r) = \sqrt{P_1+B_2^2r^2}$, and $H_2(r) = \sqrt{P_2-B_2^2r^2}$. This critical condition indicates that the contact area, surface tension, hydrostatic pressure difference, cell height, and force should satisfy Eq. S48 at the critical point.

We also find that the critical cell height $\tilde{H}_c$ increases with decreasing cantilever stiffness $\tilde{k}$ (Fig. S7), which indicates that the spontaneous rupture region shrinks as the stiffness of the cantilever decreases (Fig. 3(b) and Fig. 3(d)). Since the spontaneous rupture region shifts right as the critical cell height, H_c, increases.

Notice that the membrane tension increases rapidly when cell begins to rupture and the corresponding curves are almost vertical, i.e., the time derivative of membrane tension is diverging (green curves in Fig. S9(e) and Fig. S10(e)). This means the the time derivative of cellular surface area is also diverging, since the membrane tension is proportional to the cellular surface area (Eq. (S24)). Cells can dynamically enter "rupture" because the cell volume changes with time (see Fig. S8, S9 and S10). Even though the cell surface (cortical layer and membrane layer) can provide resistance to the stretch induced by adhesion, the membrane tension continues to increase with time as the cell spreads between the adhesive surface and cantilever. Once the membrane tension or the cell height increases to the critical value determined by Eq. (S48), the cell would not be able to bear such a high tension, and the cell would rupture and it results in a sharp decrease in stretch force (green curves in Fig. S9(a) and Fig. S10(a)). Mathematically, it indicates

that there is a critical tension or cell height beyond which no catenoid-like solution exists (Powers et al., 2002). This is similar to the spontaneous rupture of red blood cells due to the high tension induced by strong adhesion (Hategan et al., 2003). Therefore, we denote this phenomenon as "spontaneous rupture".

IV. SUPPLEMENTARY RESULTS

A. Dynamic adhesion of cells (supplementary figures to the Fig. 3 in the main text)

We only show several variables during the dynamic adhesion of cells in the Fig. 3 of the main text. Here we show how other variables evolve with time (see Fig. S8, Fig. S9, and Fig. S10).

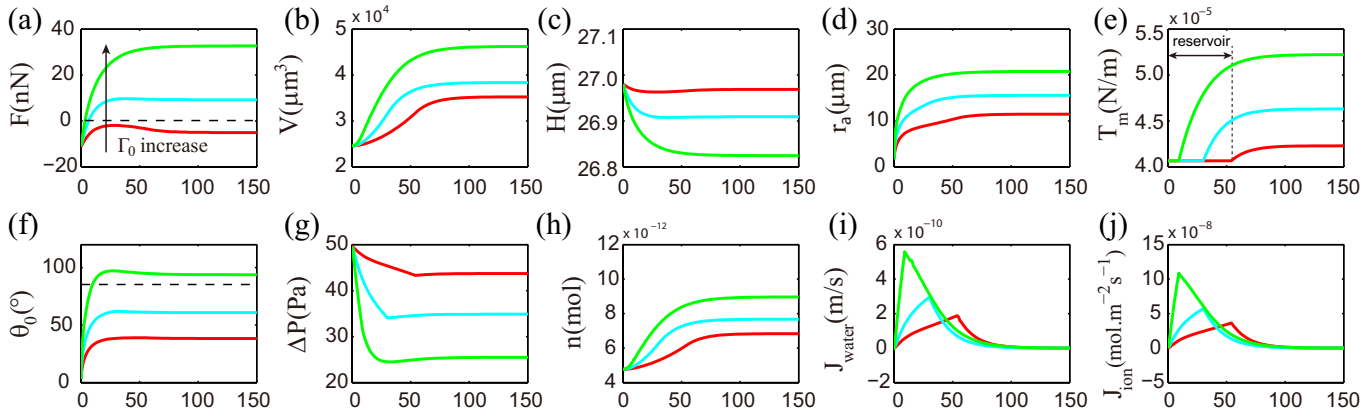

FIG. S8 Dynamic adhesion of cells adhered to an adhesive surface and a cantilever, with $r_0 = 18\mu m$ and $k = 0.5N/m$. (a) The external force, (b) cellular volume, (c) cell height, (d) adhesion radius, (e) membrane tension, (f) the contact angle, (g) hydrostatic pressure differences, (h) ions number, (i) the flux of water, and (j) the flux of ions. The red, light blue and light green curves represent the dynamic process of reaching the three stable states: (1) cell is convex ($\theta_0 < 90^o$) and $F < 0$; (2) cell is convex and $F > 0$; (3) cell is concave ($\theta_0 > 90^o$) and $F > 0$. The dash lines in (a) and (f) indicate the lines of $F = 0$ and $\theta = 90^o$, respectively.

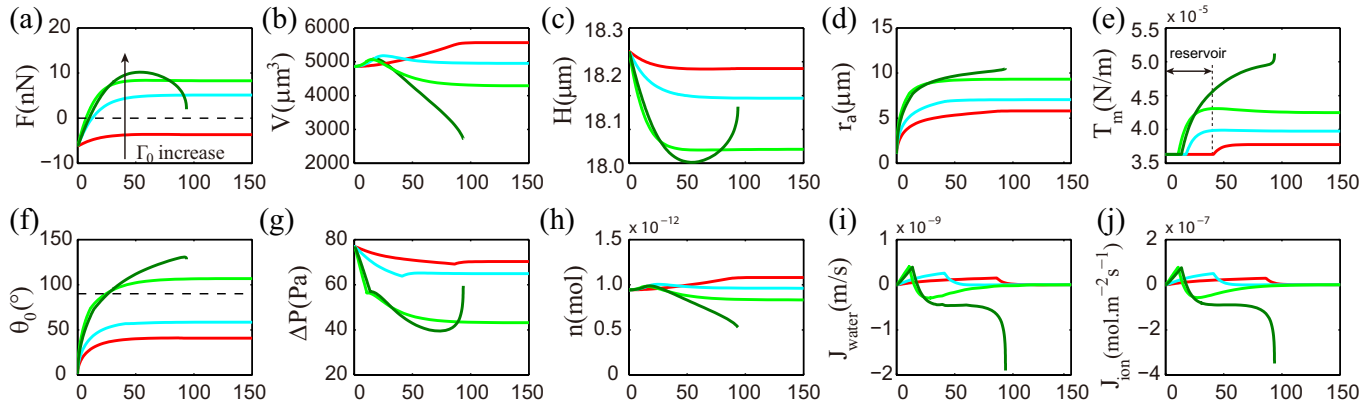

FIG. S9 Dynamic adhesion of cells adhered to an adhesive surface and a cantilever, with $r_0 = 10.5\mu m$ and $k = 0.5N/m$. (a) The external force, (b) cellular volume, (c) cell height, (d) adhesion radius, (e) membrane tension, (f) the contact angle, (g) hydrostatic pressure differences, (h) ions number, (i) the flux of water, and (j) the flux of ions. The red, light blue and light green curves represent the dynamic process of reaching the three stable states: (1) cell is convex ($\theta_0 < 90^o$) and $F < 0$; (2) cell is convex and $F > 0$; (3) cell is concave ($\theta_0 > 90^o$) and $F > 0$. The dark green curves represent the process of spontaneous rupture of cells. The dash lines in (a) and (f) indicate the lines of $F = 0$ and $\theta = 90^o$, respectively.

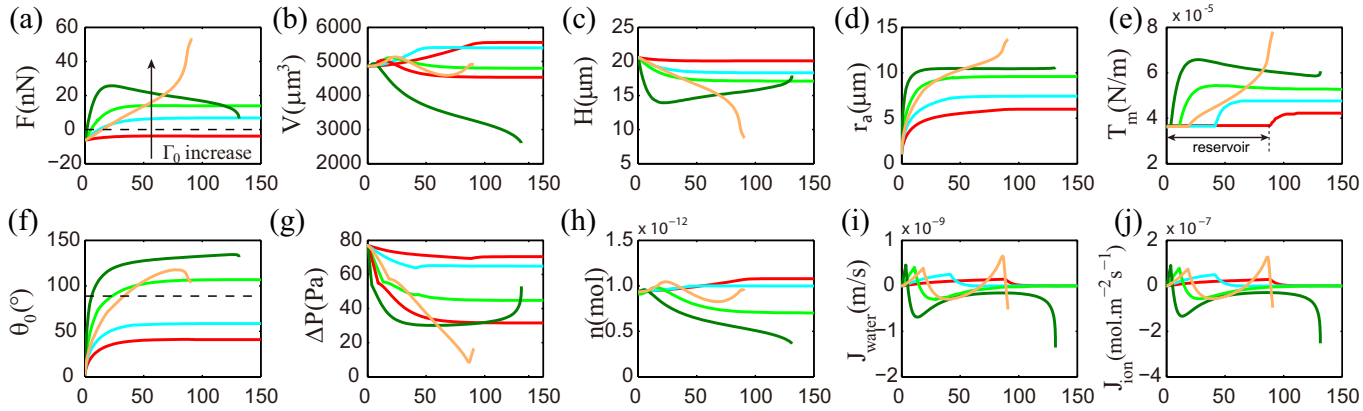

FIG. S10 Dynamic adhesion of cells adhered to an adhesive surface and a cantilever, with $r_0 = 10.5\mu m$ and $k = 0.01N/m$. (a) The external force, (b) cellular volume, (c) cell height, (d) adhesion radius, (e) membrane tension, (f) the contact angle, (g) hydrostatic pressure differences, (h) ions number, (i) the flux of water, and (j) the flux of ions. The red, light blue and light green curves represent the dynamic process of reaching the three stable states: (1) cell is convex ($\theta_0 < 90^o$) and $F < 0$; (2) cell is convex and $F > 0$; (3) cell is concave ($\theta_0 > 90^o$) and $F > 0$. The dark green and orange curves represent the processes of spontaneous rupture and collapse of cells. The dash lines in (a) and (f) indicate the lines of $F = 0$ and $\theta = 90^o$, respectively.

B. The phase diagrams of cell shapes when cellular volume and pressure are constant.

To keep the cell volume constant, we assume the membrane permeability rates to water and ion are suddenly decreased to zero so that water and ion exchange between cell and environment is stopped. Therefore, we obtain $dV/dt = 0$ and $dn/dt = 0$ from Eq. (S14) and (S15). From these equations, we get $V = V_0$ and $n = n_0$, where V_0 and n_0 are the cell volume and ion number of the initial spherical cell, respectively. Furthermore, before the membrane permeability rates to water and ion are suddenly decreased to zero, we have $dV/dt = -\alpha(\Delta P - \Delta\Pi) = 0$ in equilibrium. Therefore, we obtain the hydrostatic pressure difference as $\Delta P = \Delta\Pi = n_0 RT/V_0 - \Pi_{out}$, where R is the gas constant, T is the absolute temperature, and Π_{out} is the osmotic pressure outside the cell. After the membrane permeability rates are decreased to zero, we assume the expression of ΔP remains unchanged. Since the cell volume V and ion number n are constant, the hydrostatic pressure difference ΔP is also constant.

As shown in Fig. S11, when the cellular volume and pressure are constant during the dynamic spreading of cell, the cells would not spontaneously rupture or collapse. In this case, the cell is very hard to become concave when the stiffness of the cantilever is small (the green region in Fig. S11 (c) and (d) is small).

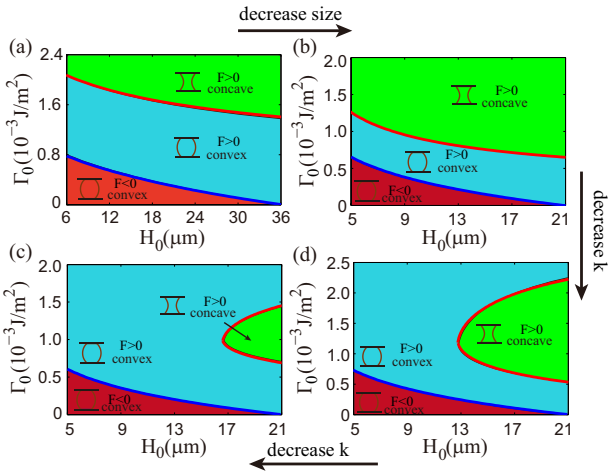

FIG. S11 The phase diagrams of cell shapes when the cellular volume and pressure are constant during the dynamic spreading of cells. (a) $r_0 = 18\mu m$ and $k = 0.5N/m$, (b) $r_0 = 10.5\mu m$ and $k = 0.5N/m$, (c) $r_0 = 10.5\mu m$ and $k = 0.005N/m$, (d) $r_0 = 10.5\mu m$ and $k = 0.01N/m$. The cells would not spontaneously rupture or collapse.

C. Dynamic detachment of convex cells with negative initial F

In the main text, we find that after the cells achieves their equilibrium adhesion state, the dynamic detachments of convex and concave cells are very different. But when the cell is convex, there are two stable states with positive F or negative F. However, we find that the detachment processes of these two kinds of convex cells are qualitatively the same as shown in Fig. S12.

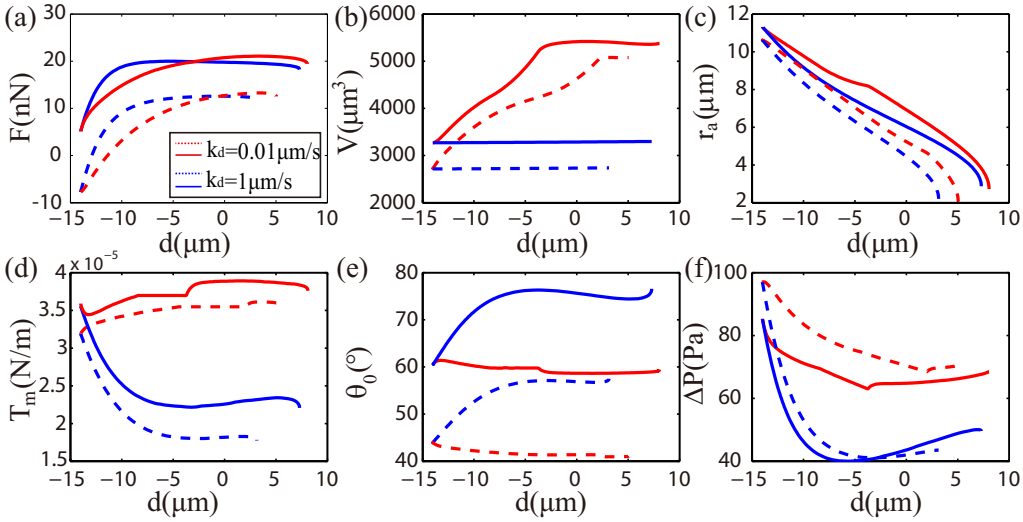

FIG. S12 Dynamic detachments of convex cells whose initial F is negative (dash curves) or positive (solid curves). (a) The external force, (b) cellular volume, (c) adhesion radius, (d) membrane tension, (e) contact angle, and (f) hydrostatic pressure differences versus the displacement of the fixed end of the cantilever $d(t)$ with various loading speed k_d.

V. THE RANGES OF PARAMETERS

In Table S1, we have discussed the range of the parameters we used in the simulation based on experimental data. In the phase diagram of cell shapes (Fig. 3 in the main text), we found that other variables, such as the stiffness of cantilever k, cell size r_0, the separation of the adhesive surface and cantilever H_0, and adhesion energy density Γ_0, are very important control parameters. Therefore, here we further discuss the realistic ranges of these parameters.

The adhesion energy density Γ_0 used in the phase diagram is in the range of $0 \sim 10^{-3} J/m^2$, which covers the range of the adhesion energy density used in experiments (around $10^{-4} J/m^2$) (Colbert et al., 2009, 2010; Chu et al., 2005). In our simulation, the cell diameter $2r_0$ is $21\mu m$ and $36\mu m$, and the separation of the adhesive surface and cantilever H_0 is smaller than $2r_0$. This is consistent with the fact that the cell diameter $2r_0$ is around tens of microns in the experiments (Fouchard et al., 2014; Fischer-Friedrich et al., 2016; Chaudhuri et al., 2009; Stewart et al., 2013; Webster et al., 2014; Thoumine and Ott, 1997; Desprat et al., 2005; Mitrossilis et al., 2009).

Based on the phase diagrams in Fig. 3 of the main text, it can be found that the unstable states are only shown when the cell is small. Therefore, to avoid the unstable states, one should use big cells for the measurements. In the case of small cells, the spontaneous rupture only appears when the separation of the adhesive surface and cantilever H_0 is big and the stiffness of the cantilever k is small. In contrast, the collapse of cell occurs when the cantilever is very soft.

In Fig. 3(a) and (b), we use $k = 0.5N/m$, which is consistent with the order of the stiffness of atomic force microscope cantilever (around $0.1N/m$) used in the experiments (Fischer-Friedrich et al., 2016; Chaudhuri et al., 2009; Stewart et al., 2013; Webster et al., 2014). In contrast, in Fig. 3(c) and (d), we use $k = 0.005N/m$ and $k = 0.01N/m$, which corresponds to the microplates manipulation experiments where the stiffness of the flexible microplate k is on the order of 0.001–0.01 N/m (Fouchard et al., 2014; Thoumine and Ott, 1997; Desprat et al., 2005; Mitrossilis et al., 2009). Especially, when the flexible microplate is too soft, the cell height can decrease almost to zero when a cell spreads between a flexible microplate and a rigid microplate (Mitrossilis et al., 2010). The stiffness of flexible microplate in their experiment is $0.005N/m$, which is the value we used in Fig. 3(c).

VI. THE QUANTITATIVE COMPARISONS WITH EXPERIMENTS

As shown in Fig. S13, we quantitatively compare the results of our model with three typical experiments, i.e., the spreading of cells adhered between two surfaces (Fig. S13(I) and (II)), cell compression (Fig. S13(III)), and cell detachment (Fig. S13(IV)).

For the comparisons with these experimental results, we only change the stiffness of cantilever k, the initial compression of cell d_0, the adhesion energy density Γ_0, the unloaded dissociation rate of receptor-ligand pair k_{off}^0, the cell size r_0 (regulated by the reference radius r_e), and the membrane elastic modulus E_m to fit these experimental results, since they are different in these experiments. In contrast, other parameters in Table S1 (Supplementary Material) are fixed.

In Fig. S13(I), we compare the dynamic adhesion results of our model with the experimental results when a cell spreads between two microplates (Fouchard et al., 2014). In these experiments, both the contact radius, R_c, and the traction force exerted on cell increase with time during the spreading of cell (Fig. S13(I)). For the solid lines in Fig. S13(I), the fitting parameters are $\Gamma_0 = 5.24 \times 10^{-3} J/m^2$, $k_{off}^0 = 0.028/s$, and $k = 12.5nN/\mu m$. Other parameters are shown in Table S1. Notice that, the stiffness of the cantilever, k, in our simulations are the same as the stiffness of the microplates in their experiment (Fouchard et al., 2014).

As shown in Fig. S13(II), during the dynamic spreading of the cell between the cantilever beam of AFM and a flat surface, the cell height first decreases and then increases, while the absolute value of the traction force exerted on the cell first increases and then decreases (Chaudhuri et al., 2009). These are similar to the results of the spontaneous rupture in our paper (red curves). In this case, the fitting parameters are $\Gamma_0 = 2.2 \times 10^{-3} J/m^2$, $k = 0.017N/m$, $r_e = 8.2\mu m$, $E_m = 90kPa$, and $d_0 = 2.3\mu m$.

In Fig. S13(III), we compare the compression results of our model with the results of the compression experiment carried out with microplates. In this experiment, cell was compressed to $12\mu m$ in 10 s (Thoumine and Ott, 1997). It was found that the cell would shorten as it is compressed in the experiment. At the same time, the compression force first increases and then relax to an equilibrium value within 20 minutes. As confirmed by our simulation results (red lines in Fig. S13III), this relaxation may be induced by the efflux of water and ions. The fitting parameters for this experiment are $r_e = 6.5\mu m$, $E_m = 314kPa$, $L_p = 4 \times 10^{-11} m/(Pa.s)$, $\Gamma_0 = 1 \times 10^{-7} J/m^2$, $k_{off}^0 = 0.01/s$,

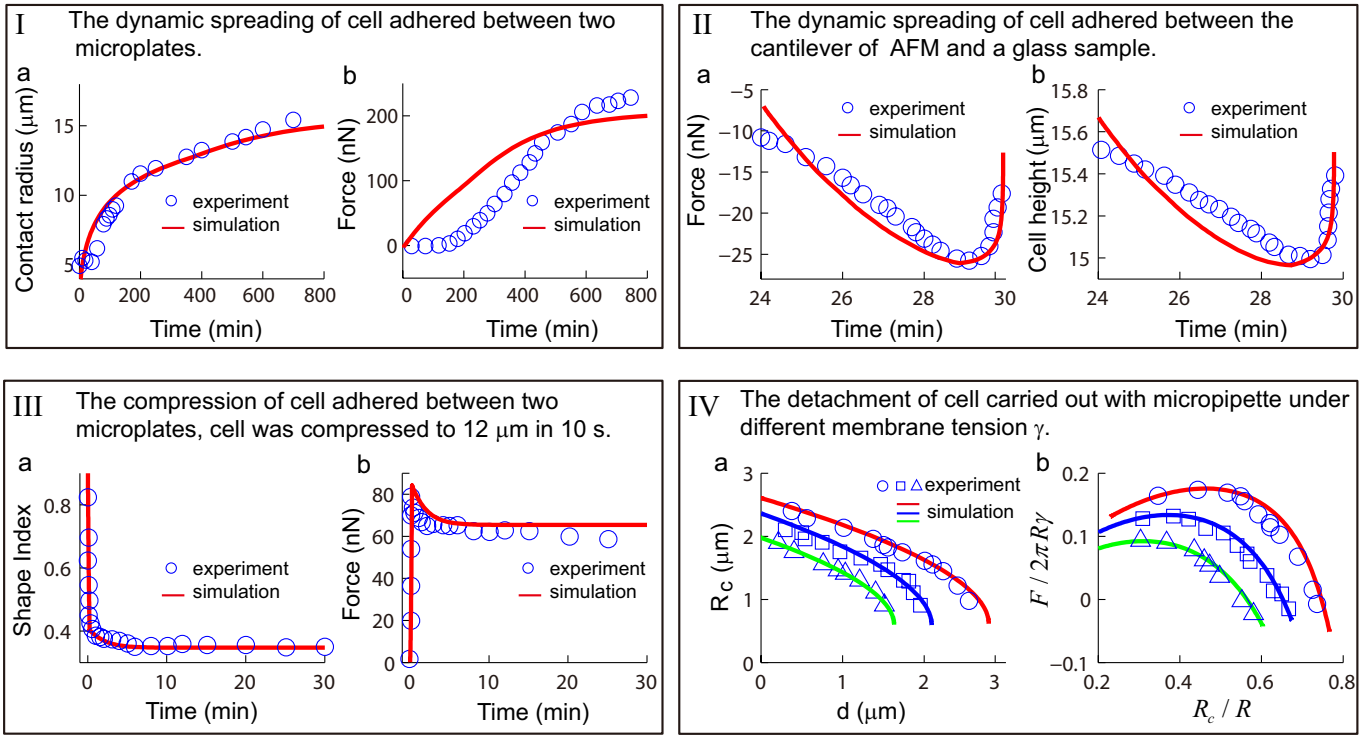

FIG. S13 The quantitative comparisons with experiments. The experimental data are adapted from (I) (Fouchard et al., 2014); (II) (Chaudhuri et al., 2009); (III) (Thoumine and Ott, 1997); (IV) (Pierrat et al., 2004). The shape index in (III) is defined as the ratio of cell height to the cell width at the equatorial center. In (IV), R_c is the contact radius, R is the radius at the equatorial center, d is the displacement of micropipette, F is the traction force exerted on cell, and γ is the membrane tension of cell.

$k = 0.01N/m$, and $d_0 = 12\mu m$. Notice that, we also change the rate constant of water transport, L_p, in this comparison, since we need to regulate the time scale of relaxation.

In the detachment experiments carried out with micropipette aspiration (Fig. S13(IV)), the authors showed that the detachment results of cell under different membrane tension γ, i.e., for different suction pressure (Pierrat et al., 2004). In our simulation, we change the initial compression distance of cell, d_0, to fit these results. The fitting parameters for this experiment are $k = 50N/m$, $\Gamma_0 = 7.4 \times 10^{-5} J/m^2$, $k^0_{off} = 0.01/s$. Furthermore, $d_0 = 1.7\mu m$ for the triangular curves, $d_0 = 2.1\mu m$ for the square curves, and $d_0 = 2.9\mu m$ for the circular curves. Notice that, in the detachment experiment carried out with micropipette aspiration, the cell is held firmly by the micropipette tip so that we use a very high cantilever stiffness $k = 50N/m$ to fit the experimental data. And the contact radius between the cell and the micropipette is assumed to be constant as proposed by a previous model (Lin and Freund, 2007).

TABLE S1 Parameters used in the simulations

parameter	description	value (Ref)
h_c	Thickness of cortical layer (nm)	400 (Tinevez et al., 2009)
h_m	Thickness of membrane layer (nm)	5 (Mitra et al., 2004)
E_m	Elastic modulus of membrane (kPa)	100 (Hochmuth and Mohandas, 1972)
b	The exponential constant of the reservoir model	2
A_c/A_s	Reservoir size	1.1(Figard and Sokac, 2014)
η	Viscosity of cortical layer ($Pa \cdot s$)	5000 (Evans and Yeung, 1989)
σ_a	Active stress of actin cortex (Pa)	400 (Hui et al., 2014)
σ_c	Threshold stress of MS channels (Pa)	900
σ_s	Saturating stress of MS channels (Pa)	4000
$\Delta\Pi_c$	Critical osmotic pressure difference of ions pump (GPa)	30
Π_{out}	Osmotic pressure outside the cell (MPa)	0.5 (Tinevez et al., 2009)
r_e	Reference radius of cell (μm)	8
L_p	Rate constant of water transport ($m.s^{-1}Pa^{-1}$)	10^{-9}
β	Rate constant of ions flux across MS channels ($mol.m^{-2}.s^{-1}Pa^{-2}$)	2×10^{-11}
γ	Rate constant of ions flux across ion pump ($mol.m^{-2}.s^{-1}Pa^{-1}$)	10^{-17} (Larsen et al., 2007)
a	The characteristic length of the bond (nm)	1 (Thoumine and Meister, 2000)
k_BT	Thermal energy ($pN.nm$)	4 (Erdmann and Schwarz, 2004)
V_e	Rupture energy of single bond ($pN.nm$)	40 (Freund, 2009)
k^0_{off}	Unloaded dissociation rate (s^{-1})	0.01 (Thoumine and Meister, 2000)

References

M. Yoneda, J. exp. Biol **41**, 893 (1964).
E. A. Evans, R. Skalak, and S. Weinbaum, *Mechanics and thermodynamics of biomembranes* (1980).
E. Fischer-Friedrich, A. A. Hyman, F. Jülicher, D. J. Müller, and J. Helenius, Scientific reports **4** (2014).
S. Sukharev, B. Martinac, V. Y. Arshavsky, and C. Kung, Biophysical Journal **65**, 177 (1993).
H. Jiang and S. X. Sun, Biophysical journal **105**, 609 (2013).
J. Dai and M. P. Sheetz, Biophysical journal **77**, 3363 (1999).
A. Diz-Muñoz, D. A. Fletcher, and O. D. Weiner, Trends in cell biology **23**, 47 (2013).
D. Raucher and M. P. Sheetz, Biophysical journal **77**, 1992 (1999).
L. Figard and A. M. Sokac, Bioarchitecture **4**, 39 (2014).
B. Sinha, D. Köster, R. Ruez, P. Gonnord, M. Bastiani, D. Abankwa, R. V. Stan, G. Butler-Browne, B. Vedie, L. Johannes, et al., Cell **144**, 402 (2011).
A. J. Kosmalska, L. Casares, A. Elosegui-Artola, J. J. Thottacherry, R. Moreno-Vicente, V. González-Tarragó, M. Á. Del Pozo, S. Mayor, M. Arroyo, D. Navajas, et al., Nature communications **6** (2015).
R. Hochmuth and N. Mohandas, Journal of biomechanics **5**, 501 (1972).
R. M. Hochmuth, N. Mohandas, and P. Blackshear Jr, Biophysical journal **13**, 747 (1973).
E. A. Evans, Methods in enzymology **173**, 3 (1989).
L. Picas, F. Rico, and S. Scheuring, Biophysical journal **102**, L01 (2012).
R. Rand, Biophysical journal **4**, 303 (1964).
R. Hochmuth and R. Waugh, Annual review of physiology **49**, 209 (1987).
E. Evans and A. Yeung, Biophysical journal **56**, 151 (1989).
A. R. Bausch, W. Möller, and E. Sackmann, Biophysical journal **76**, 573 (1999).
E. J. Koay, A. C. Shieh, and K. A. Athanasiou, Journal of biomechanical engineering **125**, 334 (2003).
A. R. Bausch, F. Ziemann, A. A. Boulbitch, K. Jacobson, and E. Sackmann, Biophysical journal **75**, 2038 (1998).
O. Thoumine and J.-J. Meister, European Biophysics Journal **29**, 409 (2000).

M.-J. Colbert, A. Raegen, C. Fradin, and K. Dalnoki-Veress, The European Physical Journal E **30**, 117 (2009).
M.-J. Colbert, F. Brochard-Wyart, C. Fradin, and K. Dalnoki-Veress, Biophysical journal **99**, 3555 (2010).
Y.-S. Chu, S. Dufour, J. P. Thiery, E. Perez, and F. Pincet, Physical review letters **94**, 028102 (2005).
G. I. Bell et al., Science **200**, 618 (1978).
Y. Lin and L. Freund, International journal of solids and structures **44**, 1927 (2007).
J. Fouchard, C. Bimbard, N. Bufi, P. Durand-Smet, A. Proag, A. Richert, O. Cardoso, and A. Asnacios, Proceedings of the National Academy of Sciences **111**, 13075 (2014).
H. Jiang, G. Huber, R. A. Pelcovits, and T. R. Powers, Physical Review E **76**, 031908 (2007).
H. Chen, T. Tang, and A. Amirfazli, Soft matter **10**, 2503 (2014).
T. R. Powers, G. Huber, and R. E. Goldstein, Physical Review E **65**, 041901 (2002).
A. Hategan, R. Law, S. Kahn, and D. E. Discher, Biophysical journal **85**, 2746 (2003).
E. Fischer-Friedrich, Y. Toyoda, C. J. Cattin, D. J. Müller, A. A. Hyman, and F. Jülicher, Biophysical Journal **111**, 589 (2016).
O. Chaudhuri, S. H. Parekh, W. A. Lam, and D. A. Fletcher, Nature methods **6**, 383 (2009).
M. P. Stewart, A. W. Hodel, A. Spielhofer, C. J. Cattin, D. J. Müller, and J. Helenius, Methods **60**, 186 (2013).
K. D. Webster, W. P. Ng, and D. A. Fletcher, Biophysical journal **107**, 146 (2014).
O. Thoumine and A. Ott, Journal of cell science **110**, 2109 (1997).
N. Desprat, A. Richert, J. Simeon, and A. Asnacios, Biophysical journal **88**, 2224 (2005).
D. Mitrossilis, J. Fouchard, A. Guiroy, N. Desprat, N. Rodriguez, B. Fabry, and A. Asnacios, Proceedings of the National Academy of Sciences **106**, 18243 (2009).
D. Mitrossilis, J. Fouchard, D. Pereira, F. Postic, A. Richert, M. Saint-Jean, and A. Asnacios, Proceedings of the National Academy of Sciences **107**, 16518 (2010).
S. Pierrat, F. Brochard-Wyart, and P. Nassoy, Biophysical journal **87**, 2855 (2004).
J.-Y. Tinevez, U. Schulze, G. Salbreux, J. Roensch, J.-F. Joanny, and E. Paluch, Proceedings of the National Academy of Sciences **106**, 18581 (2009).
K. Mitra, I. Ubarretxena-Belandia, T. Taguchi, G. Warren, and D. M. Engelman, Proceedings of the National Academy of Sciences **101**, 4083 (2004).
T. Hui, Z. Zhou, J. Qian, Y. Lin, A. Ngan, and H. Gao, Physical review letters **113**, 118101 (2014).
E. H. Larsen, N. Møbjerg, and R. Nielsen, Comparative Biochemistry and Physiology Part A: Molecular & Integrative Physiology **148**, 101 (2007).
T. Erdmann and U. Schwarz, Physical review letters **92**, 108102 (2004).
L. Freund, Proceedings of the National Academy of Sciences **106**, 8818 (2009).